錐切除で治癒的に切除ができる．進展した場合には不正出血が自覚症状であることが多く，治療としては進展度に応じた手術切除，あるいは放射線療法が行われる．ヒューマン・パピローマ・ウイルスに対するワクチンがわが国でも認可され，発症の低下を期待して接種が拡まったが，意識消失，歩行障害などの副作用が報告されたため，接種が事実上行われなくなっている．

2)　子宮体がん

子宮体がんは，子宮内膜から発生するので子宮内膜がんとも呼ばれる．女性ホルモンの1つであるエストロゲンにより増殖が刺激されるタイプとそうでないものがある．高閉経年齢，未出産，肥満が主な危険因子である．不正出血，下腹部痛が主な症状で，診断には子宮の奥まで器材を挿入し組織を採取する必要がある．いわゆる「子宮がん検診」では子宮体がんを早期発見することはできない．治療は手術，放射線療法が主であり，化学療法は進行期に主に施行され，進行の度合いによって切除範囲が拡がっていく．早期であり，子宮を摘出したくない患者には，ホルモン療法も施行される場合がある．

3)　卵巣がん

卵巣がんは初期では自覚症状はなく，進行すると下腹部圧迫感，頻尿などの腫大による圧迫症状，転移による腹水貯留症状などの自覚症状が現れるので，受診して診断されることが多い．初期は卵巣の薄い皮膜内に留まっているが，増大し一度皮膜を破ると腹腔と遮る組織がないためすぐに腹腔内に転移を起こしやすい．しかし，早期発見を効率よく行える検診システムは確立されているとはいえない．診断のための検査は，超音波検査，CT，MRIと腫瘍マーカーであるCA125の測定が一般的に行われる．

治療法は外科手術と化学療法が主体である．早期は手術で治癒的切除が可能であるが，進行した場合には手術と化学療法を組み合わせた治療が行われる．卵巣がんは固形がんの中では比較的化学療法に反応するが，化学療法は標準療法が定まっており，これに則り施行することが大切である．シスプラチンあるいはカルボプラチンの白金系抗がん剤とパクリタキセルあるいはドセタキセルのタキサン系の抗がん剤の併用療法が第1選択療法とされている．この第1選択療法の最終投与から6カ月以内の不応・再発は予後不良とされている．副作用としては，白血球減少・血小板減少，嘔気・嘔吐，脱毛は必発であり，アレルギー症状や痺れや痛みを呈する末梢神経障害がタキサン系の副作用としてみられることがある．

サイコロジストへのメッセージ

がんの種類は多く，それぞれにおいて症状，治療法および予後が大きく異なり，1つの臓器から複数の種類のがんが発生することも多い．本項で取り上げることのできなかった他のがんについては他書を参考していただくしかないが，症状（QOLとも密接に関連する）と予後が患者の心理状態に大きな影響を及ぼす．また，選択できる標準療法があとどれくらい存在するのか，あるいは，もう選択肢がないのか，また，どの治療法を選択すべきなのかという点により，患者の心理状態に与えるインパクトは大きく異なることに留意が必要である．

I 第2章 絶対に必要な医学の知識
第12節 がん関連の臨床研究

長村文孝

はじめに

がんは，わが国において死亡原因の約1/3を占める．また，固形がんにおいては，局所の浸潤，あるいは転移により手術で十分に切除できない時等の化学療法の効果は，ほとんどの場合，生存期間の延長もしくは生活の質（quality of life：QOL）の向上であり，治癒は期待できない．近年，分子標的療法が出現し，旧来の殺細胞性の抗がん剤よりも副作用が軽減される傾向にあるが，がん以外の疾患に用いる薬剤と比較すると，副作用は一般的に高度である．このような状況を背景として，より有効な，あるいはより副作用の軽い治療方法を開発することが，「がん」の治療開発として急務である．そのため，新たな治療法開発・検証を目指した「臨床研究」あるいは「臨床試験」が盛んに行われている．

1．「臨床研究」，「臨床試験」とは

「臨床研究」とは，人を対象として，疾病の予防方法，診断方法および治療方法の改善，疾病原因および病態の理解並びに患者のQOLの向上を目的として実施される医学系研究である（厚生労働省「臨床研究に関する倫理指針」の「用語の定義」を改変）．これには，手術で摘出された検体，保存されている血清やDNAあるいは診療情報を用いた研究も含まれる．「臨床試験」は，「臨床研究」のうち，医薬品の投与あるいは医療機器を用いる等の被験者に対する介入行為を伴う研究であり，通常は研究計画を立て，実施計画書（プロトコール）の作成後に実施される（図1）．「治験」は，「臨床試験」のうち，医薬品

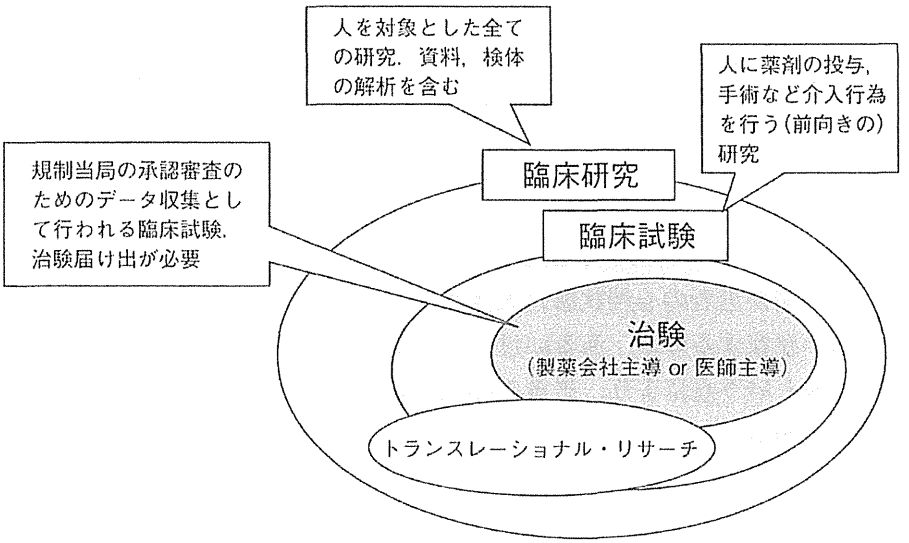

図1　臨床研究の分類

あるいは医療機器の厚生労働省等の規制当局からの製造・販売の認可を得るためのデータ収集を目的として行われる「臨床試験」を指し，試験開始に先立ち，わが国では医薬品医療機器総合機構（Pharmaceuticals and Medical Devices Agency：PMDA）を通じて厚生労働大臣宛に治験届けが提出され，PMDAで審査が行われる．「治験」は製薬企業等が主体のものと，医師が「自ら」実施する「医師主導治験」がある．後者は，対象患者数が少ないために製薬企業等が適応拡大等の治験を意図しない場合や，医師が研究者として自ら開発した治療法について承認申請を念頭に置き実施する場合に大別される．

「治験」ではない「臨床試験」は「自主臨床試験」あるいは「非治験臨床試験」等と呼ばれる．近年，なぜがんが発症するのか，あるいはがん細胞と正常細胞の違いは何か等の基礎研究が急速に発達し，これらの成果を基に臨床試験を行う「トランスレーショナルリサーチ（translational research：TR）」が盛んに行われるようになり，新たな治療法の開発として期待されている．TRは一般に早期の臨床試験に限定することが多く，「橋渡し研究」あるいは「探索型臨床研究」とも呼ばれる．抗がん剤の有効性，あるいは副作用の個人差等の臨床の結果を遺伝情報として研究することも多いが，このような臨床の結果から基礎に戻って行う研究もリーバースTRと呼称され，TRに含まれることがある．

2．臨床研究とガイドライン等

臨床研究の倫理的規範として，世界医師会が策定した「ヘルシンキ宣言」が知られている．研究参加のためのインフォームド・コンセント（informed consent：IC）の手続き，実施計画書の作成，倫理審査委員会での承認等，実施するための原則等から構成されている．他の法令や指針，あるいはガイドラインの憲法的存在となっていて，これを規範として臨床研究あるいは臨床試験の種類に対応して法規，指針等が定められている．

臨床研究・臨床試験には，その実施を定める法令やガイドラインが存在する．「治験」は薬事法とその関連省令に拠って規定されている．「治験」を規定する省令は「医薬品の臨床試験の実施の基準に関する省令」であり，英名が“Good Clinical Practice”であるので略して「GCP」と呼ばれることが多い．ヒトゲノムや遺伝子解析の臨床研究は「ヒトゲノム・遺伝子研究に関する倫理指針」によって規定され，治験ではない遺伝子治療は「遺伝子治療臨床研究に関する指針」により，治験以外の再生医療臨床試験は「ヒト幹細胞を用いた臨床研究に関する指針」により，観察研究等の疫学研究は「疫学研究に関する倫理指針」により規定されている．前述以外の臨床研究・臨床試験は「臨床研究に関する倫理指針」により広くカバーされている．

3．がんにおける予防の臨床試験

がんの発症には遺伝，環境，食事，薬物，物理的刺激等多くの要素が関与する．がんの発症予防の研究は「疫学研究」として，がんの発症の危険度を高める（あるいは低下させる）要因が何であるかを多数の患者の資料を基に解析されることが多い．疫学研究から，受動喫煙を含めた喫煙が肺がんだけではなく，口腔・咽頭・食道・膵臓・腎臓等多くのがんの発症リスクであることが判明した．このようなものには，B型肝炎ウイルス・C型肝

炎ウイルス感染による肝がんの発症，肥満における結腸がん，膵がん，閉経後乳がんなどが示されている．このように蓄積したデータの解析から危険因子の発見がなされるが，この危険因子が本当にがんの発症に関わっているのかを実証することは現実には非常に大変である．過去にはコーヒーが発がんの危険因子とされていたが，実際にはコーヒーの摂取は発がんのリスクではなかったことが判明したこともある．ヘリコバクター・ピロリ菌の場合では，除菌群と非除菌群の比較を前向き試験（prospective study）として試験計画を立案し，被験者を募集して実施する必要があるが，非常に多数の被験者と長期間の観察が必要であること，多額の研究資金が必要であること，リスクを参加者が認識していた場合には，それを回避する可能性があることから，臨床試験として実施することは困難な場合も多い．

がんでは，治療による副作用の発症予防の臨床試験も存在する．たとえば，化学療法後の口内炎予防のケア（例：ブラッシングの教育の成果）など高度な医療を用いなくとも実施できるテーマは多く存在し，また，心理面接の導入や面談等の工夫により，罹病によるうつ状態の改善や，前向きな心理状態への改善等を研究することも考えられる．

4．がん診断の臨床試験

診断の場合には，血液や尿等の検体の解析を基にするものと，画像診断等の医療機器に関するものとに大別される．尿や便を使用する場合は体への侵襲はなく，採血の場合には侵襲性は低く，倫理的判断をあまり要しないことが多い．しかし，被曝等の副作用の可能性のある医療機器を使用する場合や，ラジオ・アイソトープを体内に注射し放射線の被曝を受ける場合等では，安全性・有益性の十分な検討と被験者へ適切なICが必須となる．

5．がんの治療法の臨床試験

治療においても，過去のデータを基に推察する「臨床研究」と新たに介入行為を行う「臨床試験」に大別されるが，一般的には後者を指す．また，医薬品等の投与と手術等の手技においては「臨床試験」の概念がやや異なる．医薬品の臨床試験は第一相試験から第三相試験まで分類され，新薬開発では第一相試験から行われる．第一相試験は，動物実験等による非臨床試験での結果を基に，人への投与量，投与経路，投与スケジュール等を十分に検討した後に，人に初めて投与する段階である．抗がん剤以外の医薬品では，安全性，薬効の有無および薬理学的な情報の収集を目的として，健常人あるいは軽症の患者を対象として行われる．一方，抗がん剤の第一相試験は対象が異なり通常生存期間を延長する標準療法の無い段階の患者，すなわち標準療法の無くなった段階の患者を対象として行う．また，投与量を段階的に増加する用量漸増試験として行われ，人に投与できる最大耐用量（maximum tolerated dose：MTD）を決定する試験デザインであることが多い．これは，抗がん剤は，① 副作用が強い場合や，催奇性や2次発がんの危険性により健常人あるいは長期生存が見込まれる患者に投与することは倫理的に許容できない場合が多いこと，② 一般に抗がん剤は有効性と安全性を考慮した至適投与量の幅が狭く，有効性の低い低投与群あるいは毒性の強い高投与群の被験者が存在し，治療としての恩恵にあずかる

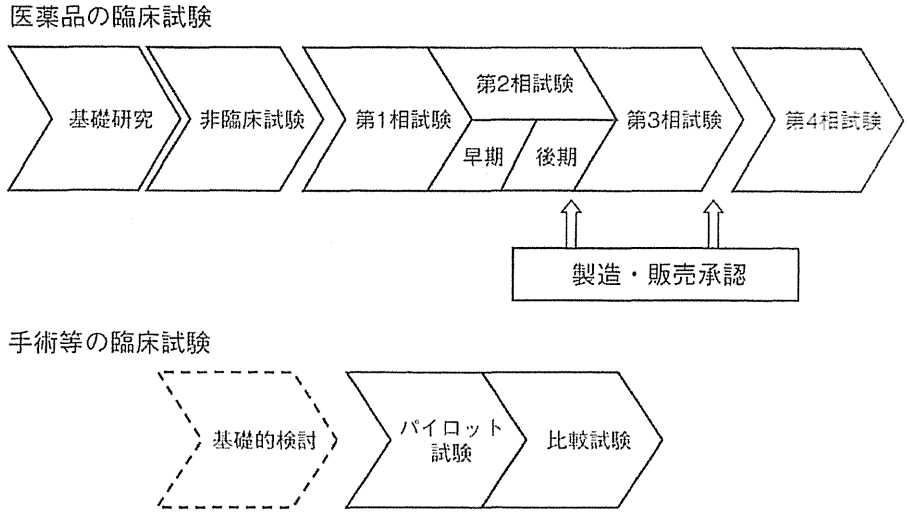

図2　臨床試験の流れ

ことのできる可能性のない被験者，あるいは毒性が強く生命の危機が生じる可能性のある被験者も存在することによる．これらを背景として，第一相試験は，被験者に有効性をもたらす可能性は低い．しかしながら，治癒の可能性を信じている患者も多いことに留意する必要がある．第二相試験は，第一相試験の結果を基に投与量・投与スケジュールを決定した後に，数十人程度の患者に投与し，有効性・安全性のある程度の情報を得ることを目的とする．1つの薬剤を単一投与量で最初の第二相試験を行うことが多いが，投与量の比較あるいは標準薬との比較試験として行われることある．また，「第二相試験」として行われる場合と，「早期第二相試験」と「後期第二相試験」とに分けて行われる場合がある．第三相試験は，標準療法との比較による有効性・安全性の検証を目的として数百人規模で実施される．迅速な第三相試験の実施と承認を目的として，最近は国際共同治験も増えている．第四相試験は市販後に情報を収集するために行われる．手術などの手技の臨床試験では，試験の分類が細分化されておらず，新たな手法を探索的に検討するパイロット試験と標準手技との比較試験に大別される（図2）．

臨床試験では，試験の目的を具体的数値で評価するためにエンドポイントを設定する．がんにおいては，最終的な目的は生存期間の延長あるいはQOLの向上であるが，これらを評価するためには多くの被験者と長い期間を必要とする．したがって，早期の試験では，これらと因果関係を有すると考えられる奏功率（腫瘍が縮小した被験者の割合）をサロゲート（代替）・エンドポイントとして用いることが多い．

サイコロジストへのメッセージ

臨床研究，特に臨床試験においては，被験者に対する十分な説明と適切な同意の取得が必須である．そのためには試験の目的，方法の理解が必要であり，更にその背景の理解として，対象とするがんの知識も必要となる．臨床試験が対象とするがんの種類，段階，予後，比較試験の場合には，その対象となる治療法等により患者の不安，選択への迷い，あるいは過度の期待が懸念されるので十分な知識をもって接することが重要である．

Biochemical and Biophysical Research Communications 437 (2013) 185–191

Contents lists available at SciVerse ScienceDirect

Biochemical and Biophysical Research Communications

journal homepage: www.elsevier.com/locate/ybbrc

Conditional loss of heparin-binding EGF-like growth factor results in enhanced liver fibrosis after bile duct ligation in mice

Takayo Takemura [a,1], Yuichi Yoshida [a,1], Shinichi Kiso [a,*], Takashi Kizu [a], Kunimaro Furuta [a], Hisao Ezaki [a], Mina Hamano [a], Mayumi Egawa [a], Norihiro Chatani [a], Yoshihiro Kamada [a], Yasuharu Imai [b], Shigeki Higashiyama [c], Ryo Iwamoto [d], Eisuke Mekada [d], Tetsuo Takehara [a]

[a] Department of Gastroenterology and Hepatology, Osaka University, Graduate School of Medicine, Osaka, Japan
[b] Department of Gastroenterology, Ikeda Municipal Hospital, Ikeda, Osaka, Japan
[c] Department of Biochemistry and Molecular Genetics, Ehime University, Graduate School of Medicine and Department of Cell Growth and Tumor Regulation, Proteo-Medicine Research Center (ProMRes), Ehime University, Shitsukawa, Toon, Ehime, Japan
[d] Department of Cell Biology, Research Institute for Microbial Diseases, Osaka University, Suita, Osaka, Japan

ARTICLE INFO

Article history:
Received 6 May 2013
Available online 4 June 2013

Keywords:
Bile duct ligation
Heparin-binding EGF-like growth factor
Hepatic stellate cells
Liver fibrosis
Transforming growth factor-β

ABSTRACT

Our aims were to evaluate the involvement of heparin-binding EGF-like growth factor (HB-EGF) in liver fibrogenesis of humans and mice and to elucidate the effect of HB-EGF deficiency on cholestatic liver fibrosis using conditional HB-EGF knockout (KO) mice. We first demonstrated that gene expression of HB-EGF had a positive significant correlation with that of collagen in human fibrotic livers, and was increased in bile duct ligation (BDL)-induced fibrotic livers in mouse. We then generated conditional HB-EGF knockout (KO) mice using the interferon inducible *Mx-1* promoter driven Cre recombinase transgene and wild type (WT) and KO mice were subjected to BDL. After BDL, KO mice exhibited enhanced liver fibrosis with increased expression of collagen, compared with WT mice. Finally, we used mouse hepatic stellate cells (HSCs) to examine the role of HB-EGF in the activation of these cells and showed that HB-EGF antagonized TGF-β-induced gene expression of collagen in mouse primary HSCs. Interestingly, HB-EGF did not prevent the TGF-β-induced nuclear accumulation of Smad3, but did lead to stabilization of the Smad transcriptional co-repressor TG-interacting factor. In conclusion, our data suggest a possible protective role of HB-EGF in cholestatic liver fibrosis.

© 2013 Elsevier Inc. All rights reserved.

1. Introduction

Chronic liver injury and wound healing response result in the accumulation of extracellular matrix (ECM) and the replacement of normal parenchyma by scar tissue, causing liver fibrosis and cirrhosis [1,2]. In fibrotic livers, hepatic stellate cells (HSCs) are known to be a key player in producing ECM [1,2]. The activation of HSCs has been shown to be caused by a variety of cytokines or growth factors, including TGF-β or PDGF, during the liver fibrosis process [1,2]. Among these factors, the role of epidermal growth factor receptor (EGFR) ligands in this process has been poorly understood.

The heparin-binding epidermal growth factor-like growth factor (HB-EGF) belongs to the EGF family of growth factors and associates with and stimulates EGF receptors (EGFR) and EerbB4 [3,4]. HB-EGF has been shown to be synthesized as a type 1 transmembrane protein (pro HB-EGF) [3,5]. Cleavage of membrane anchored pro HB-EGF at the juxtamembrane domain results in the shedding of mature HB-EGF (soluble HB-EGF) [6]. Soluble HB-EGF has a mitogenic effect on several cell types, such as vascular smooth muscle cells, fibroblasts and keratinocytes [3,4]. Previously, we reported that HB-EGF has a capacity to stimulate hepatocyte proliferation both *in vitro* and *in vivo* [7,8]. We have also reported that HB-EGF was induced during liver regeneration after partial hepatectomy [9] and that hepatocyte-specific HB-EGF transgenic mouse showed accelerated proliferation of hepatocytes during liver regeneration after partial hepatectomy [10]. Because abnormal liver regeneration is known to be associated with liver fibrosis, we hypothesized that loss of HB-EGF may affect liver fibrosis during chronic liver injury. Recently, it has been reported that traditional

Abbreviations: ALT, alanine aminotransferase; ALP, alkaline phosphatase; BDL, bile duct ligation; EGF, epidermal growth factor; H&E, hematoxylin and eosin; HB-EGF, heparin-binding EGF-like growth factor; HSCs, hepatic stellate cells; KO, knockout; poly I:C, polyinosinic:polycytidylic acid; RT-PCR, reverse-transcription polymerase chain reaction; T.Bil, total bilirubin; TGF-β, transforming growth factor-β; TNF-α, tumor necrosis factor-α; WT, wild type.

* Corresponding author. Address: Department of Gastroenterology and Hepatology, Osaka University, Graduate School of Medicine, 2-2 K1 Yamadaoka, Suita, Osaka 565-0871, Japan. Fax: +81 6 6879 3629.
E-mail address: kiso@gh.med.osaka-u.ac.jp (S. Kiso).

[1] These authors equally contributed to this paper.

0006-291X/$ - see front matter © 2013 Elsevier Inc. All rights reserved.
http://dx.doi.org/10.1016/j.bbrc.2013.05.097

HB-EGF KO mice showed enhanced liver fibrosis in chemical-induced liver fibrosis [11]. However, the role of HB-EGF in cholestatic liver fibrosis remains unclear.

Because HB-EGF null mice die immediately after birth due to severe heart failure [12], we recently generated conditional HB-EGF knockout mice using the interferon-inducible Mx1-Cre transgene and examined the role of HB-EGF during toxin-induced acute liver injury [13]. In the present study, we investigated the role of HB-EGF in cholestatic liver fibrosis using these conditional HB-EGF KO mice.

2. Materials and methods

2.1. Human liver tissues

Non-tumorous liver tissues were obtained from 16 patients undergoing partial liver section at Ikeda Municipal Hospital, Japan. The degree of liver fibrosis was classified as F0 (absent), F1 (portal fibrosis), F2 (portal fibrosis with few septa), F3 (septal fibrosis), or F4 (cirrhosis). Detailed information of the patients is presented in the Supplemental Information. Informed consent was obtained from all patients and the study was approved by the Ethical Committees of Osaka University Hospital and Ikeda Municipal Hospital.

2.2. Mice

Generation of C57BL/6 mice carrying the HB-EGF gene flanked by loxP sites (HB-EGF$^{lox/lox}$ mice) was described previously [12]. HB-EGF$^{lox/lox}$ mice were further bred with Mx1-Cre transgenic (TG) C57BL/6 mice (Jackson Laboratories, West Grove, PA, USA) to generate Mx1-Cre HB-EGF$^{lox/lox}$ mice. To delete HB-EGF from the liver, Mx1-Cre HB-EGF$^{lox/lox}$ (KO) mice and HB-EGF$^{lox/lox}$ (WT) mice were injected with 250 μg of polyinosinic:polycytidylic acid (poly I:C) (P1530 Sigma, St. Louis, MO) intraperitoneally three times at 2-day intervals as previously described [13]. The experimental protocol was approved by the Ethics Review Committee for Animal Experimentation of Osaka University, Graduate School of Medicine.

2.3. Bile duct ligation model

To induce liver fibrosis, male 8–10-week-old WT and KO mice underwent bile duct ligation (BDL) [14]. The BDL procedure was performed as previously described. In brief, the common bile duct was doubly ligated under anesthesia via laparotomy. The sham procedure was performed via similar laparotomy without BDL.

2.4. Histological analysis

To evaluate liver fibrosis, liver sections were stained in 0.1% Sirius red F3B (Sigma–Aldrich, St. Louis, MO, USA) in saturated aqueous picric acid (Sigma–Aldrich). The hematoxylin and eosin (H&E) stained liver sections were also used to evaluate oncotic necrosis. The relative fibrotic or oncotic necrosis area was calculated using ImageJ software. To evaluate macrophage infiltration in the injured livers, liver sections were stained with anti F4/80 antibody (Abcam, Cambridge, MA).

2.5. Real time RT-PCR

Total RNA was extracted from whole liver using the RNeasy Mini Kit (Qiagen, Hilden, Germany) as previously described [15]. Reverse transcription polymerase chain reaction (RT-PCR) and real-time PCR were performed as previously described [15]. The Quantitect gene assay kit (Qiagen, Hilden, Germany) was used for analysis of human HB-EGF, human Col1α1, human Col1α2, human Acta2, human TGF-β, human GAPDH, mouse HB-EGF, mouse Col1α1, mouse Col1α2, mouse Acta2, mouse TGF-β, mouse PDGF, mouse MMP13 mouse Timp1, mouse F4/80, mouse CD68, mouse TNF-α, mouse IL-6, mouse MCP-1, mouse IL-1β, and mouse GAPDH. The relative gene expression was quantified using GAPDH as an internal control.

2.6. Isolation and culture of mouse hepatic stellate cells

Mouse HSCs were isolated from male C57BL6 mice by in situ collagenase perfusion and Nycodenz (Sigma–Aldrich) density gradients as previous described [16]. Isolated HSCs were cultured at 37 °C under 5% CO_2 in Dulbecco's modified Eagle medium containing 10% FCS. Activated HSCs after a few passages were used for the experiments in this study. To assess the effect of HB-EGF on the activation of HSCs, serum-starved HSCs were stimulated with 1 ng/ml of TGF-β (100 21, PeproTech EC, Rocky Hill, CT) with or without 20 ng/ml of HB-EGF (259-HE-050, R&D Systems Inc. Minneapolis, MN) for 24 h and fibrosis related genes were examined by real time RT-PCR.

2.7. Western blotting

For extraction of nuclear protein, subcellular fractionation was performed using the NE-PERTM nuclear extraction kit (Pierce, Rockford, IL). Western blotting was performed as previously described [15]. To examine the effect of HB-EGF on the nuclear accumulation of Smad3 in HSCs, serum-starved HSCs were stimulated with 1 ng/ml of TGF-β and increasing amount of HB-EGF (0–100 ng/ml) for 40 min. To examine the effect of HB-EGF on phosphorylation of TGIF in HSCs, serum-starved HSCs were stimulated with 20 ng/ml of HB-EGF for 0–120 min. We used primary antibodies specific for Smad3 (9513, Cell Signaling, Danvers, MA), TGIF (sc-9084, Santa Cruz Biotechnology, Santa Cruz, CA), and Histone H3 (4499, Cell Signaling, Danvers, MA).

2.8. Transient reporter gene assay

HSCs were transfected with 1 μg of reporter plasmid (pGL3-$(CAGA)_9$-luc) and 100 ng of control plasmids (pGL4-RLtk) using FuGENE6 (1815091, Roche, Basel Switzerland) in 6-well plates. After incubation for 6 h, the cells were serum-starved overnight, then stimulated with 1 ng/ml of TGF-β with or without 20 ng/ml of HB-EGF for 24 h. Luciferase activity was measured with a luminometer using the Dual-Luciferase Reporter Assay System (Promega, Madison, WI). pGL3-$(CAGA)_9$-luc [17] was gifted by Dr. S. Ehata and Dr. K. Miyazono (University of Tokyo).

2.9. Statistical analysis

The results are presented as mean ± SE. Differences between two groups were examined for statistical significance using the Mann–Whitney *U* test and multiple comparisons were made by the Bonferroni/Dunn test. A p value less than 0.05 denoted the presence of a statistically significant difference.

3. Results

3.1. Increased expression of HB-EGF is associated with liver fibrosis in humans and mice

To investigate the involvement of HB-EGF in the process of liver fibrosis, we examined the gene expression of HB-EGF in the livers of patients with chronic liver disease. Real time RT-PCR analysis

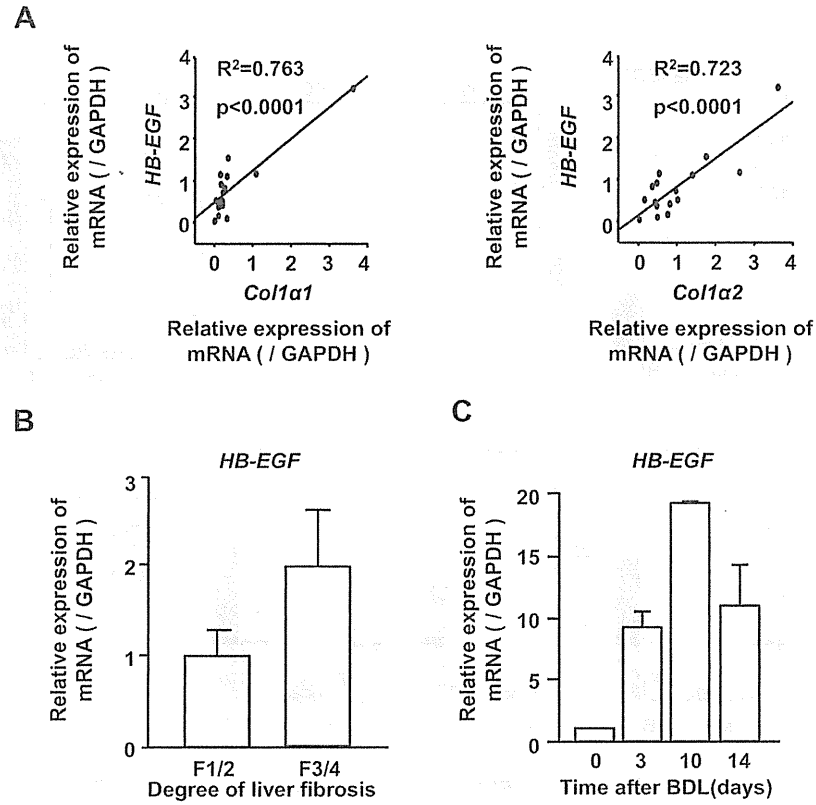

Fig. 1. Increased expression of HB-EGF gene during liver fibrosis in humans and mice. (A) Correlation between hepatic gene expression of HB-EGF and that of fibrosis-related genes, such as Col1α1 and Col1α2 in human samples with chronic liver disease. (B) Hepatic HB-EGF expression was increased as the fibrosis developed in human samples with chronic liver disease. (C) Increased expression of HB-EGF in murine livers during liver fibrosis after BDL.

showed that the expression of HB-EGF mRNA was increased in fibrotic livers and was positively correlated with that of fibrosis-related genes, such as collagen type I alpha 1 (Col1α1) and collagen type I alpha 2 (Col1α2) (Fig. 1A). We also revealed that the gene expression of HB-EGF was increased during the development of liver fibrosis in these patients (Fig. 1B) and that its expression was induced by bile duct ligation (BDL) in the mouse model (Fig. 1C). These results indicated the possible involvement of HB-EGF in liver fibrogenesis.

3.2. HB-EGF KO mice show enhanced liver fibrosis after BDL

To investigate the role of HB-EGF in liver fibrosis, we performed BDL in conditional HB-EGF knockout (KO) and wild type (WT) mice. Real time RT-PCR analysis confirmed that the expression of HB-EGF mRNA was reduced in KO mice compared with that of WT mice (Fig. 2A). KO mice exhibited about a 1.5-fold increase in the fibrosis area as evaluated by Sirius red staining compared with WT mice after BDL (Fig. 2B and C). This enhanced fibrosis in KO mice was associated with increased expression of fibrosis-related genes, such as Col1α1, Col1α2 or TIMP1, as assessed by real time RT-PCR analysis, compared with WT mice (Fig. 2D). These data indicated that loss of HB-EGF caused enhanced liver fibrosis during chronic liver injury.

3.3. HB-EGF KO mice display enhanced oncotic necrosis and macrophage infiltration in the liver after BDL

We next characterized the effect of HB-EGF deletion on the liver injury after BDL by H&E staining of liver sections. KO mice displayed significantly more oncotic necrosis after BDL than WT mice (Fig. 3A). Quantification of H&E staining showed about a 2.6-fold increase in the oncotic necrotic area in KO mice compared with WT mice after BDL (Fig. 3B).

Kupffer cells, or resident hepatic macrophages, are known to be involved in the development of liver fibrosis [2,18]. We therefore examined the effect of HB-EGF deletion on macrophage infiltration in the liver after BDL by F4/80 staining of the injured livers after BDL (Fig. 3D). KO mice showed increased infiltration of F4/80 positive macrophages in the injured livers compared with WT mice (Fig. 3D). Consistent with this, KO mice showed increased expression of F4/80 and CD68 in the injured livers compared with WT mice (Fig. 3E and F). However, there was no statistically significant difference in the hepatic expression of pro-inflammatory genes, such as TNF-α, IL-6, MCP-1 or IL-1β, between the WT and KO mice (Fig. 3G–J). These data indicate that the enhanced liver fibrosis in KO mice might not be associated with the cytokine production of macrophages in the injured livers induced by BDL.

3.4. HB-EGF attenuates TGF-β-induced expression of fibrosis-related genes in murine hepatic stellate cells

Because hepatic stellate cells (HSC) are known to play a major role in the development of liver fibrosis [2,18], we investigated the role of HB-EGF on the activation of mouse primary HSCs *in vitro*. HB-EGF treatment significantly reduced the gene expression of Col1α1 or Col1α2 in the HSCs activated by TGF-β (Fig. 4A). HB-EGF treatment also significantly suppressed TGF-β-dependent transcription and this effect was cancelled by addition of U0126, ERK1/2 inhibitor in HSCs (Fig. 4B). We therefore examined the effect of HB-EGF treatment on the nuclear accumulation of Smad3 induced by TGF-β in HSCs (Fig. 4C). However, Western

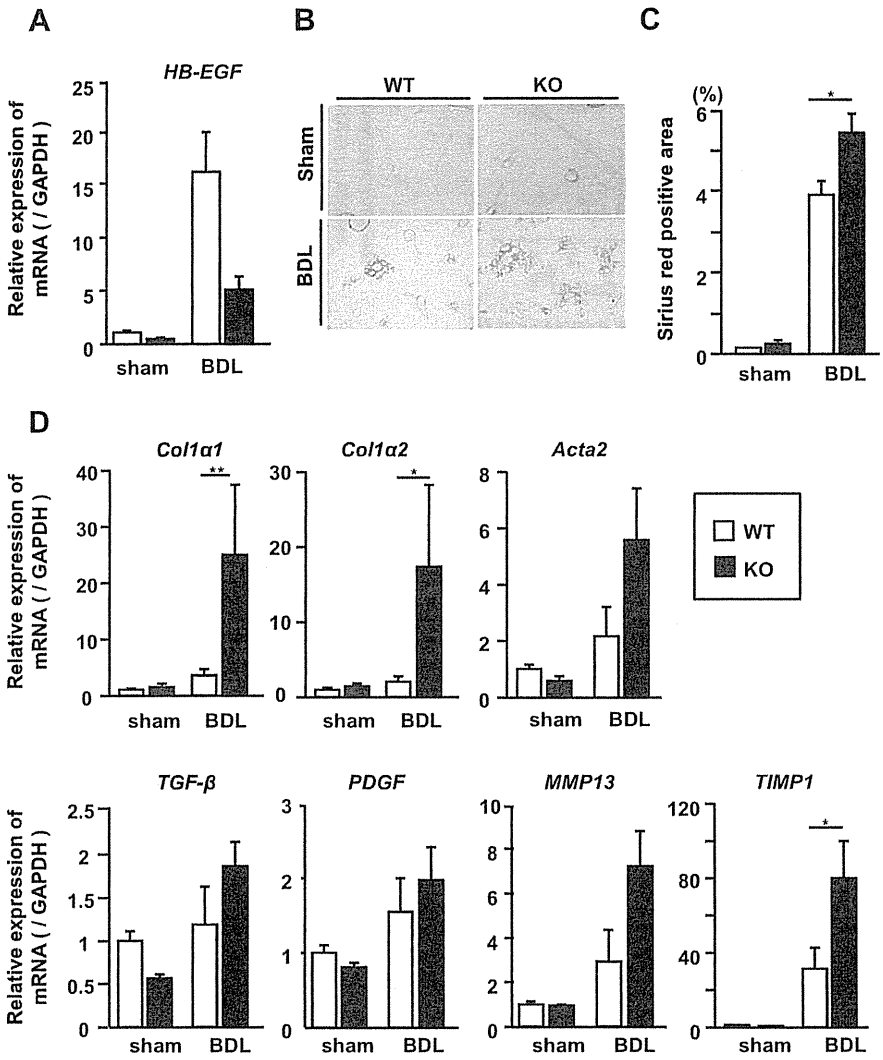

Fig. 2. Enhanced live fibrosis in conditional HB-EGF KO mice after BDL. WT and KO mice were subjected to BDL or sham operation (sham). (A) Gene expression of HB-EGF in the liver at 10 days after BDL ($n = 6$ for WT, $n = 5$ for KO) or sham ($n = 6$ for WT, $n = 5$ for KO) in WT and KO mice. (B) Representative views of Sirius red staining of the liver sections at 14 days after BDL ($n = 7$ for WT, $n = 6$ for KO) or sham (original magnification × 200). (C) Quantification of Sirius red staining positive area in the injured livers of WT and KO mice at 14 days after BDL or sham (data are mean ± SE, $^{*}p < 0.05$). (D) Gene expression of Collα1, Collα2, Acta2, TGF-β, PDGF, MMP13 and Timp1 in the liver at 10 days after BDL or sham in WT and KO mice (data are mean ± SE, $^{*}p < 0.05$, $^{**}p < 0.01$).

blotting analysis showed that HB-EGF did not decrease TGF-β-dependent nuclear accumulation of Smad3 in HSCs (Fig. 4C). Finally, we demonstrated that HB-EGF treatment caused the stabilization of Smad transcriptional co-repressor TG-interacting factor (TGIF) of HSCs (Fig. 4D). These results indicate that HB-EGF treatment may suppress the activation of HSCs through the inhibition of TGF-β signaling.

4. Discussion

EGFR ligands are known to stimulate hepatocyte proliferation and promote liver regeneration during acute liver injury [19,20]. However, their role in liver fibrogenesis remains elusive. In this study, we investigated whether conditional loss of HB-EGF could affect liver fibrosis after BDL, a well-established murine model of cholestatic liver fibrosis, using conditional HB-EGF KO mice. We demonstrated that conditional loss of HB-EGF accelerates liver fibrosis during cholestatic liver injury. Our results suggest that HB-EGF plays a protective role during cholestatic liver fibrosis.

Using liver samples from patients with chronic liver disease, we first demonstrated that the expression of HB-EGF had a positive correlation with that of fibrosis-related genes and was increased as liver fibrosis developed. The expression of HB-EGF was also increased during liver fibrosis after BDL in mice. Collectively, one explanation for our results is that the increased expression of HB-EGF during chronic liver injury might serve as a self-defense mechanism to suppress an excess fibrosis response. Consistent with our observation, previous publications also showed that hepatocyte growth factor (HGF) and its receptor, c-Met system play a protective role for liver fibrosis, although the expression of HGF increases during this process [21–23].

To investigate the molecular mechanism underlying the enhanced liver fibrosis in KO mice, we examined the liver injury and macrophage infiltration in the injured livers. Histological examinations showed larger areas of oncotic necrosis in the livers of KO mice than WT mice. This result was consistent with the result of our recent publication demonstrating that conditional HB-EGF KO mice show the increased liver injury after a single administration of CCl_4 [13]. Real time RT-PCR also showed

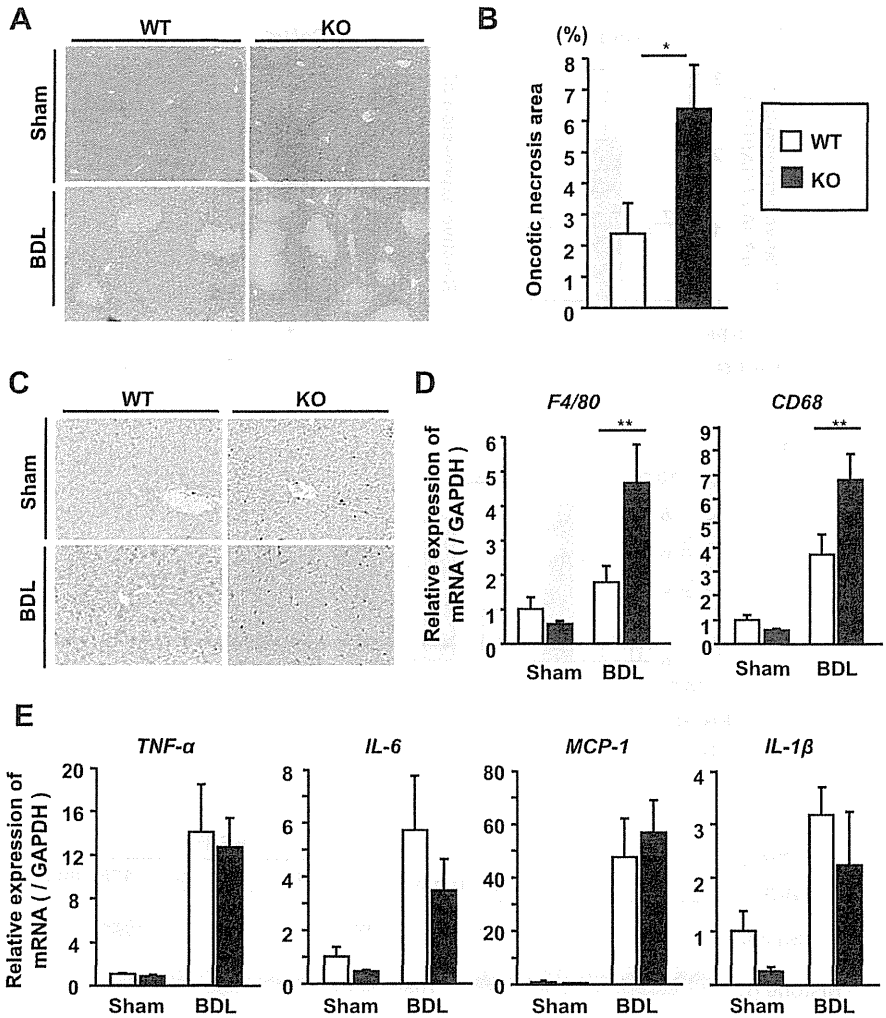

Fig. 3. Enhanced hepatic necrosis and macrophage infiltration in conditional HB-EGF KO mice after BDL. (A) Representative H&E staining of the livers of WT and KO mice at 10 days after BDL ($n = 6$ for WT, $n = 5$ for KO) or sham ($n = 6$ for WT, $n = 5$ for KO) (magnification × 100). (B) Quantification of the area of onocotic necrosis in injured livers of WT and KO mice at 10 days after BDL. (C) Representative F4/80 staining of the livers of WT and KO mice at 10 days after BDL or sham (magnification × 400). (D) Gene expression of F4/80 and CD68 in the liver at 10 days after BDL or sham in WT and KO mice. (E) Gene expression of TNF-α, IL-6, MCP-1, and IL-1β at 10 days after BDL or sham in WT and KO mice (data are mean ± SE, $^{*}p < 0.05$, $^{**}p < 0.01$).

increased expression of F4/80 or CD68, surface markers for macrophages, in the injured livers of KO mice compared with WT mice. Because non-parechymal cells, such as Kupffer cells or sinusoidal endotherial cells, were the main source of HB-EGF production in the liver, these cells might play a protective role against inflammation by the secretion of HB-EGF. However, we could not detect any difference in the gene expression of pro-inflammatory cytokines, such as TNF-α or IL-1β or that of pro-inflammatory chemokine, MCP-1. These findings raise the possibility that the loss of HB-EGF itself might affect the activation of HSCs during liver fibrosis.

Finally, we examined the effects of direct interaction of HB-EGF with HSCs, the major ECM-producing cells in the liver. We demonstrated that HB-EGF could reduce TGF-β-induced expression of Col1α1 or Col1α2 in HSCs. We also demonstrated that HB-EGF could suppress TGF-β-dependent transcription via the ERK dependent pathway in HSCs. It is interesting to note that HB-EGF did not affect the nuclear accumulation of TGF-β induced Smad3, but caused stabilization of the Smad transcriptional co-repressor TGIF of these cells. TGIF was originally identified as a Smad2 co-repressor in the TGF-β/Nodal/Activin signaling pathways [24]. EGF has been shown to phosphorylate TGIF via Ras-MAP kinase pathways, leading to the stabilization of TGIF [25]. In lung fibroblasts, EGF also has been shown to antagonize TGF-β-induced expression of tropoelastin, a component of elastic fibers, via stabilization of TGIF without preventing the nuclear accumulation of Smad2/3 by TGF-β [26]. Considering these findings and ours suggests that HB-EGF might antagonize TGF-β-induced expression fibrosis-related genes through an EGFR-TGIF signaling pathway in HSCs.

Previous work has been demonstrated that over-expression of HB-EGF in pancreatic islets resulted in pancreatic fibrosis and epithelial metaplasia [27]. These reports indicated that HB-EGF has a pro-fibrogenic potential in the pancreas. Pancreatic fibrosis is known to be associated with the activation of pancreatic stellate cells as in the case of the liver fibrosis [28]. In our study, HB-EGF suppressed the activation of HSCs, and conditional loss of HB-EGF resulted in enhanced liver fibrosis in murine cholestatic fibrosis models. It is interesting to note that the role of HB-EGF in tissue fibrosis is completely different between the liver and the pancreas and further investigation will be needed to elucidate this.

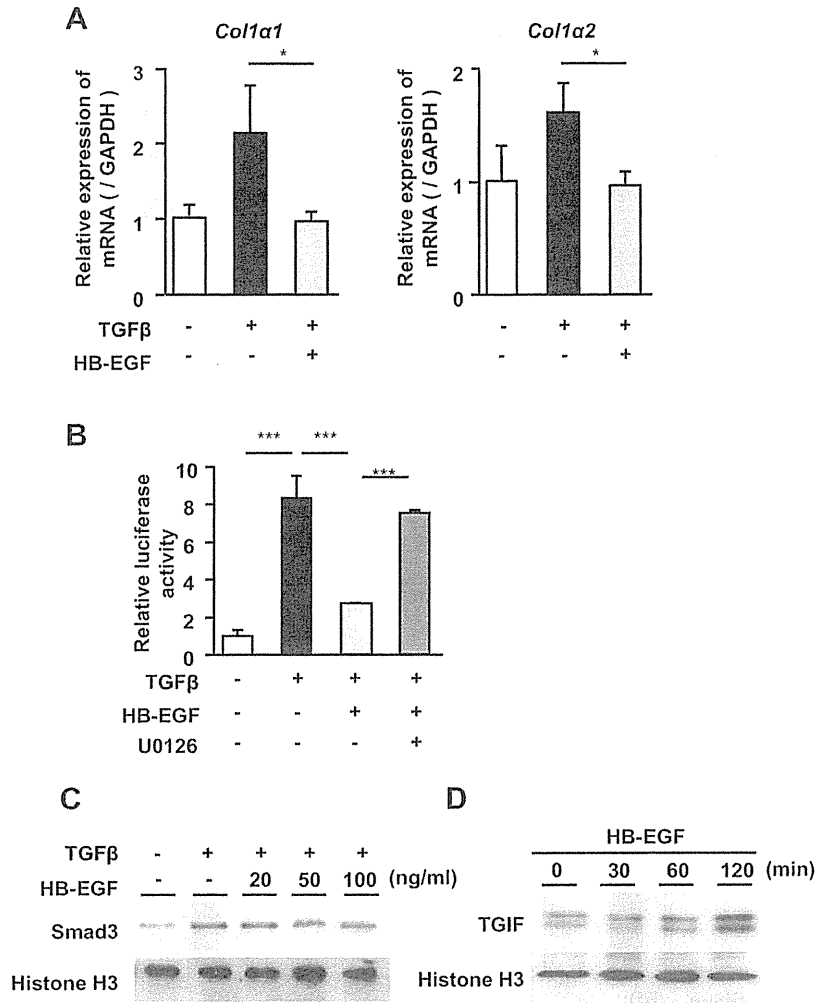

Fig. 4. HB-EGF attenuates TGF-β-induced expression of fibrosis-related genes in murine hepatic stellate cells. (A) Gene expression of Col1α1 and Col1α2 in HSCs treated with HB-EGF (data are mean ± SE, $^{*}p < 0.05$). (B) Effect of HB-EGF on TGF-β-dependent transcription in HSCs (data are mean ± SE, $^{***}p < 0.001$). (C) Effect of HB-EGF on the nuclear accumulation of Smad3 in HSCs. (D) Effect of HB-EGF on the stabilization of TGIF in HSCs.

Recently, Huang et al. published their work about the role of HB-EGF on liver fibrosis using different mouse lines and models [11]. Although they used the TAA or CCl_4-induced liver fibrosis model instead of the BDL model, our results were generally in agreement with theirs on the role of HB-EGF during liver fibrosis. In our study, we developed conditional KO mice to suppress the expression of HB-EGF in the liver because traditional HB-EGF KO mice die immediately after birth due to severe heart failure [12]. According to the original paper regarding KO mice, which they used in their fibrosis study, most of these traditional HB-EGF KO mice die before weaning and survivors have been shown to have enlarged, dysfunctional hearts and reduced life spans [29]. Thus, our conditional HB-EGF KO mice might be more suitable for examining the role of HB-EGF during liver fibrosis than traditional HB-EGF KO mice. Moreover, our results could be used to describe the inhibitory role of HB-EGF on the TGF-β-induced activation of HSCs.

In summary, we demonstrated in the present study that conditional loss of HB-EGF resulted in enhanced liver fibrosis in the murine cholestatic model and that HB-EGF suppresses the activation of HSCs. Our findings further suggest that HB-EGF might be a potential therapeutic target against liver fibrosis.

Acknowledgments

We thank Dr. S. Ehata and Dr. K. Miyazono (University of Tokyo) for providing a pGL3-$(CAGA)_9$-luc reporter plasmid. This work was supported by in part of a Grant-in-Aid for Scientific Research from the Japan Society for the Promotion of Science and a Grant from the Intractable Hepato-biliary Diseases Study Group in Japan (Health Labour Sciences Research Grant).

Appendix A. Supplementary data

Supplementary data associated with this article can be found, in the online version, at http://dx.doi.org/10.1016/j.bbrc.2013.05.097.

References

[1] S.L. Friedman, Liver fibrosis – from bench to bedside, J. Hepatol. 38 (Suppl. 1) (2003) S38–53.
[2] R. Bataller, D.A. Brenner, Liver fibrosis, J. Clin. Invest. 115 (2005) 209–218.
[3] S. Miyamoto, H. Yagi, F. Yotsumoto, T. Kawarabayashi, E. Mekada, Heparin-binding epidermal growth factor-like growth factor as a novel targeting molecule for cancer therapy, Cancer Sci. 97 (2006) 341–347.
[4] R. Iwamoto, E. Mekada, ErbB and HB-EGF signaling in heart development and function, Cell Struct. Funct. 31 (2006) 1–14.

[5] S. Higashiyama, J.A. Abraham, J. Miller, J.C. Fiddes, M. Klagsbrun, A heparin-binding growth factor secreted by macrophage-like cells that is related to EGF, Science 251 (1991) 936–939.
[6] K. Goishi, S. Higashiyama, M. Klagsbrun, N. Nakano, T. Umata, M. Ishikawa, E. Mekada, N. Taniguchi, Phorbol ester induces the rapid processing of cell surface heparin-binding EGF-like growth factor: conversion from juxtacrine to paracrine growth factor activity, Mol. Biol. Cell 6 (1995) 967–980.
[7] N. Ito, S. Kawata, S. Tamura, S. Kiso, H. Tsushima, D. Damm, J.A. Abraham, S. Higashiyama, N. Taniguchi, Y. Matsuzawa, Heparin-binding EGF-like growth factor is a potent mitogen for rat hepatocytes, Biochem. Biophys. Res. Commun. 198 (1994) 25–31.
[8] S. Kiso, S. Kawata, S. Tamura, S. Umeki, N. Ito, H. Tsushima, A. Yamada, J. Miyagawa, S. Higashiyama, N. Taniguchi, Y. Matsuzawa, Effects of exogenous human heparin-binding epidermal growth factor-like growth factor on DNA synthesis of hepatocytes in normal mouse liver, Biochem. Biophys. Res. Commun. 259 (1999) 683–687.
[9] S. Kiso, S. Kawata, S. Tamura, S. Higashiyama, N. Ito, H. Tsushima, N. Taniguchi, Y. Matsuzawa, Role of heparin-binding epidermal growth factor-like growth factor as a hepatotrophic factor in rat liver regeneration after partial hepatectomy, Hepatology 22 (1995) 1584–1590.
[10] S. Kiso, S. Kawata, S. Tamura, Y. Inui, Y. Yoshida, Y. Sawai, S. Umeki, N. Ito, A. Yamada, J. Miyagawa, S. Higashiyama, T. Iwawaki, M. Saito, N. Taniguchi, Y. Matsuzawa, K. Kohno, Liver regeneration in heparin-binding EGF-like growth factor transgenic mice after partial hepatectomy, Gastroenterology 124 (2003) 701–707.
[11] G. Huang, G.E. Besner, D.R. Brigstock, Heparin-binding epidermal growth factor-like growth factor suppresses experimental liver fibrosis in mice, Lab. Invest. 92 (2012) 703–712.
[12] R. Iwamoto, S. Yamazaki, M. Asakura, S. Takashima, H. Hasuwa, K. Miyado, S. Adachi, M. Kitakaze, K. Hashimoto, G. Raab, D. Nanba, S. Higashiyama, M. Hori, M. Klagsbrun, E. Mekada, Heparin-binding EGF-like growth factor and ErbB signaling is essential for heart function, Proc. Natl. Acad. Sci. USA 100 (2003) 3221–3226.
[13] T. Takemura, Y. Yoshida, S. Kiso, Y. Saji, H. Ezaki, M. Hamano, T. Kizu, M. Egawa, N. Chatani, K. Furuta, Y. Kamada, R. Iwamoto, E. Mekada, S. Higashiyama, N. Hayashi, T. Takehara, Conditional knockout of HB-EGF in the liver accelerates carbon tetrachloride-induced liver injury in mice, Hepatol. Res. 43 (2013) 238–248.
[14] E. Seki, S. De Minicis, C.H. Osterreicher, J. Kluwe, Y. Osawa, D.A. Brenner, R.F. Schwabe, TLR4 enhances TGF-beta signaling and hepatic fibrosis, Nat. Med. 13 (2007) 1324–1332.
[15] H. Ezaki, Y. Yoshida, Y. Saji, T. Takemura, J. Fukushima, H. Matsumoto, Y. Kamada, A. Wada, T. Igura, S. Kihara, T. Funahashi, I. Shimomura, S. Tamura, S. Kiso, N. Hayashi, Delayed liver regeneration after partial hepatectomy in adiponectin knockout mice, Biochem. Biophys. Res. Commun. 378 (2009) 68–72.
[16] N. Kawada, T. Kuroki, K. Kobayashi, M. Inoue, K. Nakatani, K. Kaneda, K. Nagata, Expression of heat-shock protein 47 in mouse liver, Cell Tissue Res. 284 (1996) 341–346.
[17] S. Dennler, S. Itoh, D. Vivien, P. Ten Dijke, S. Huet, J.M. Gauthier, Direct binding of Smad3 and Smad4 to critical TGF beta-inducible elements in the promoter of human plasminogen activator inhibitor-type 1 gene, EMBO J. 17 (1998) 3091–3100.
[18] J.P. Iredale, Models of liver fibrosis: exploring the dynamic nature of inflammation and repair in a solid organ, J. Clin. Invest. 117 (2007) 539–548.
[19] A. Natarajan, B. Wagner, M. Sibilia, The EGF receptor is required for efficient liver regeneration, Proc. Natl. Acad. Sci. USA 104 (2007) 17081–17086.
[20] G.K. Michalopoulos, Liver regeneration, J. Cell. Physiol. 213 (2007) 286–300.
[21] T. Cramer, D. Schuppan, M. Bauer, D. Pfander, P. Neuhaus, H. Herbst, Hepatocyte growth factor and c-Met expression in rat and human liver fibrosis, Liver Int. 24 (2004) 335–344.
[22] T. Ueki, Y. Kaneda, H. Tsutsui, K. Nakanishi, Y. Sawa, R. Morishita, K. Matsumoto, T. Nakamura, H. Takahashi, E. Okamoto, J. Fujimoto, Hepatocyte growth factor gene therapy of liver cirrhosis in rats, Nat. Med. 5 (1999) 226–230.
[23] J.L. Xia, C. Dai, G.K. Michalopoulos, Y. Liu, Hepatocyte growth factor attenuates liver fibrosis induced by bile duct ligation, Am. J. Pathol. 168 (2006) 1500–1512.
[24] D. Wotton, R.S. Lo, S. Lee, J. Massague, A Smad transcriptional corepressor, Cell 97 (1999) 29–39.
[25] R.S. Lo, D. Wotton, J. Massague, Epidermal growth factor signaling via Ras controls the Smad transcriptional co-repressor TGIF, EMBO J. 20 (2001) 128–136.
[26] S. Yang, M.A. Nugent, M.P. Panchenko, EGF antagonizes TGF-beta-induced tropoelastin expression in lung fibroblasts via stabilization of Smad corepressor TGIF, Am. J. Physiol. Lung Cell. Mol. Physiol. 295 (2008) L143–151.
[27] A.L. Means, K.C. Ray, A.B. Singh, M.K. Washington, R.H. Whitehead, R.C. Harris Jr., C.V. Wright, R.J. Coffey Jr., S.D. Leach, Overexpression of heparin-binding EGF-like growth factor in mouse pancreas results in fibrosis and epithelial metaplasia, Gastroenterology 124 (2003) 1020–1036.
[28] M.B. Omary, A. Lugea, A.W. Lowe, S.J. Pandol, The pancreatic stellate cell: a star on the rise in pancreatic diseases, J. Clin. Invest. 117 (2007) 50–59.
[29] L.F. Jackson, T.H. Qiu, S.W. Sunnarborg, A. Chang, C. Zhang, C. Patterson, D.C. Lee, Defective valvulogenesis in HB-EGF and TACE-null mice is associated with aberrant BMP signaling, EMBO J. 22 (2003) 2704–2716.

jbc The Journal of Biological Chemistry

AFFINITY SITES

ASBMB
American Society for Biochemistry and Molecular Biology

Cell Biology:

Metastasis Suppressor Tetraspanin CD82/KAI1 Regulates Ubiquitylation of Epidermal Growth Factor Receptor

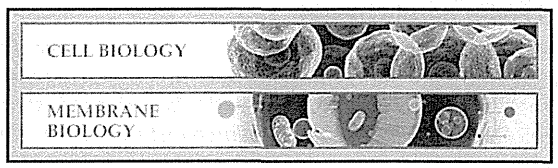

Elena Odintsova, Guillaume van Niel, Hélène Conjeaud, Graça Raposo, Ryo Iwamoto, Eisuke Mekada and Fedor Berditchevski

J. Biol. Chem. 2013, 288:26323-26334.
doi: 10.1074/jbc.M112.439380 originally published online July 29, 2013

Access the most updated version of this article at doi: 10.1074/jbc.M112.439380

Find articles, minireviews, Reflections and Classics on similar topics on the JBC Affinity Sites.

Alerts:
- When this article is cited
- When a correction for this article is posted

Click here to choose from all of JBC's e-mail alerts

Supplemental material:
http://www.jbc.org/content/suppl/2013/07/29/M112.439380.DC1.html

This article cites 45 references, 16 of which can be accessed free at
http://www.jbc.org/content/288/36/26323.full.html#ref-list-1

Downloaded from http://www.jbc.org/ at OSAKA UNIVERSITY on May 1, 2014

THE JOURNAL OF BIOLOGICAL CHEMISTRY VOL. 288, NO. 36, pp. 26323–26334, September 6, 2013
© 2013 by The American Society for Biochemistry and Molecular Biology, Inc. Published in the U.S.A.

Metastasis Suppressor Tetraspanin CD82/KAI1 Regulates Ubiquitylation of Epidermal Growth Factor Receptor*[S]

Received for publication, July 10, 2013, and in revised form, July 25, 2013 Published, JBC Papers in Press, July 29, 2013, DOI 10.1074/jbc.M112.439380

Elena Odintsova[‡1], **Guillaume van Niel**[§], **Hélène Conjeaud**[¶], **Graça Raposo**[§], **Ryo Iwamoto**[‖], **Eisuke Mekada**[‖], **and Fedor Berditchevski**[‡]

From the [‡]*School of Cancer Sciences, College of Medical and Dental Sciences, University of Birmingham, Birmingham B15 2TT, United Kingdom, the* [§]*Institut Curie, Centre de Recherche, and Unité Mixte de Recherche 144, Centre National de la Recherche Scientifique, F-75248 Paris, France, the* [¶]*Matière et Systèmes Complexes, UMR 7057 CNRS, Université Denis Diderot Paris-VII, 75205 Paris, France, and the* [‖]*Research Institute for Microbial Diseases, Osaka University, Osaka 565-0871, Japan*

Background: Tetraspanin CD82/KAI1 is associated with EGF receptor and regulates its signaling.
Results: CD82 controls ubiquitylation of EGF receptor after stimulation with heparin-binding ligands and alters receptor trafficking.
Conclusion: CD82 regulates communication between heparan sulfate proteoglycans and ligand-bound EGFR, thus affecting the activity of c-Cbl.
Significance: Lateral cross-talk initiated by CD82-dependent interactions is critical for modulation of EGFR function.

Ligand-induced ubiquitylation of EGF receptor (EGFR) is an important regulatory mechanism that controls endocytic trafficking of the receptor and its signaling potential. Here we report that tetraspanin CD82/KAI1 specifically suppresses ubiquitylation of EGFR after stimulation with heparin-binding EGF or amphiregulin and alters the rate of recruitment of the activated receptor to EEA1-positive endosomes. The suppressive effect of CD82 is dependent on the heparin-binding domain of the ligand. Deletion of the C-terminal cytoplasmic domain of CD82 (CD82ΔC mutant) inhibits endocytic trafficking of the tetraspanin and compromises its activity toward heparin-binding EGF-activated EGFR. Reduced ubiquitylation of EGFR is accompanied by PKC-dependent increase in serine phosphorylation of c-Cbl in cells expressing elevated levels of CD82. Furthermore, phosphorylation of threonine 654 (PKC phosphorylation site) in the juxtamembrane domain of the receptor is considerably increased in CD82-expressing cells. These results describe previously unsuspected links between tetraspanin proteins and ubiquitylation of their molecular partners (*e.g.*, EGFR). Our data identify CD82 as a new regulator of c-Cbl, which discriminatively controls the activity of this E3 ubiquitin ligase toward heparin-binding ligand-EGFR pairs. Taken together, these observations provide an important new insight into the modulatory role of CD82 in endocytic trafficking of EGF receptor.

Tetraspanins comprise a family of four transmembrane domains proteins that function as the main structural components and organizers of specific microdomains: tetraspanin-enriched microdomains (TERM).[2] Within TERM, tetraspanins link together various receptors and cytoplasmic signaling molecules and regulate lateral cross-talk at the plasma membrane (1–3). In addition, there is growing evidence that tetraspanins have a role in trafficking, sorting in endosomes and exocytosis of the molecules associated with TERM (4). However, endocytic trafficking routes for the majority of tetraspanins and the molecular mechanisms underlying their role in endocytic trafficking of associated partners remain largely unknown.

Metastasis suppressor tetraspanin CD82/KAI1 has been implicated in the modulation of activities of various transmembrane receptors such as EGFR, c-Met, and β1 integrins (5–11). Specifically, we have previously shown that elevated expression of CD82 in epithelial cells results in the increased internalization rate of EGFR, thus attenuating the signaling of the receptor (5). A more recent report described the involvement of CD82 in controlling EGFR diffusion in the plasma membrane and its interaction with the machinery of clathrin-dependent endocytosis (12). Likewise, there is evidence that CD82 regulates surface levels of α6β1 integrin by accelerating its ligand-dependent internalization (7). Previously described modulatory activities of CD82 were directed toward the cell surface pool of the associated receptors. Indeed, until recently, the intracellular distribution of CD82 has been studied mainly in hematopoetic cells, where it was shown to be abundant in multivesicular bodies in B lymphocytes (13) and in endolysosomal tubules in dendritic cells (14). In their recent report Xu *et al.* (15) confirmed that in prostate epithelial cells CD82 is localized to various endocytic organelles including late endosomes and lysosomes. They also showed that CD82 is internalized via clathrin- and dynamin-independent pathways (15). However, neither the intracellular pathways of internalized CD82 nor the

* This work was supported by Breast Cancer Campaign Grants 2008MaySP18, 2007PR22, and 2003:712 (to E. O. and F. B.).
[S] This article contains supplemental Fig. S1.
[1] To whom correspondence should be addressed: School of Cancer Sciences, College of Medical and Dental Sciences, University of Birmingham, Edgbaston, Birmingham B15 2TT, UK. Tel.: 44-121-4151043; Fax: 44-121-4144486; E-mail: e.odintsova@bham.ac.uk.

[2] The abbreviations used are: TERM, tetraspanin-enriched microdomain; EGFR, EGF receptor; HB-EGF, heparin-binding EGF; AR, amphiregulin; EEA1, early endosomal antigen 1; HSPG, heparan sulfate proteoglycans; PM, plasma membrane.

Downloaded from http://www.jbc.org/ at OSAKA UNIVERSITY on May 1, 2014

involvement of this tetraspanin in postendocytic trafficking of its associated proteins has been investigated in previous studies.

The level and duration of EGFR signaling is determined by a variety of factors, not the least by the post-translational modifications initiated by ligand binding (16). Different ligands induce diverse cellular responses and may result in different outcomes for the receptor (17).

In this study we have found that CD82 reduces the level of ubiquitylation of EGFR following stimulation with HB-EGF and AR. Heparin-binding domain of the ligand is essential for CD82-induced changes in the ubiquitylation of the receptor. Moreover, this correlates with delayed HB-EGF-induced phosphorylation of EGFR on Tyr^{1045}, the recruitment point for c-Cbl to the receptor. Changes in ubiquitylation may be correlated with the activation of PKC because phosphorylation of Thr^{654} on EGFR (main PKC phosphorylation site) is increased in CD82-expressing cells. Furthermore, increase in serine phosphorylation of c-Cbl is PKC-dependent in CD82-expressing cells. We also found that a reduced level of ubiquitylation of EGFR resulted in diversification of its postendocytic trafficking route. Specifically, we established that CD82 alters kinetics of the recruitment of ligand-stimulated receptor to early endosomes and egress from these compartments. Importantly, these activities of CD82 toward EGFR are dependent on the C-terminal cytoplasmic region of the tetraspanin. Thus, this study has established a new paradigm for tetraspanin-dependent regulation of postendocytic trafficking of their associated receptors.

EXPERIMENTAL PROCEDURES

Mutagenesis and Viral Transduction—The mutant of CD82 (CD82ΔC) with the last 11 amino acids (HSEDYSKVPKY) deleted for this study was generated by a standard PCR protocol (sequences of the primers are available upon request). Stable transfectants of HB2 cells with mutant and wild type CD82 were generated by using retroviral transduction. First, FLY A13 packaging cells were transfected with the plasmid containing appropriate cDNA by using Lipofectamine (Invitrogen) according to the manufacturer's protocol. Five days later, the medium was harvested for use as a "transient virus." Second, HB2 cells were infected overnight with various dilutions of virus. After 3 days, the puromycin selection was started. The puromycin-resistant colonies were pooled together and sorted by flow cytometry with an anti-CD82 mAb (IA4).

2.5.2A cells depleted of CD82 were generated using MISSION shRNA library (Sigma) following the manufacturer's protocol. Successful clones were selected in puromycin-containing medium.

Cell Lines, Antibodies, and Reagents—Human mammary epithelial cells HB2 and 2.5.2A (18) wild type cells were maintained in DMEM (Invitrogen) supplemented with 10% FCS, 10 μg/ml of hydrocortisone, and 10 μg/ml of insulin. HB2/CD82wt, HB2/CD82ΔC, and 2.5.2A/shCD82 (3) cells were propagated in the same medium supplemented with puromycin (2 μg/ml).

The anti-CD82 mAb M104 was kindly provided by Dr. O. Yoshie. The anti-CD82 mAb TS82b was kindly provided by Dr. E. Rubinstein. We are grateful to Professor M. Marsh for providing anti-CD63 mAb (1B5). Anti-EGFR mAbs (Ab-16, Ab-15, and Ab-12) were purchased from ThermoScientific (Lab Vision). Anti-c-Cbl polyclonal antibody was purchased from R&D Systems, and anti-c-Cbl mAb (A-9) was from Santa Cruz. Anti-phosphoserine polyclonal antibody was from Abcam. Anti-phospho-c-Cbl (Tyr^{774} and Tyr^{331}) and anti-phospho-EGFR (Tyr^{1068} and Tyr^{1045}) rabbit monoclonal antibodies were purchased from Cell Signaling Technology. Anti-phospho-EGFR (Thr^{654}) antibody (clone 3F2) was purchased from Millipore. Anti-EEA1 mAb was from Transduction Lab. Mono- and polyubiquitinylated conjugates, mouse mAb (clone FK2) was purchased from Enzo Life Sciences. All Alexa Fluor-conjugated secondary antibodies for immunofluorescence were purchased from Molecular Probes, Invitrogen/Life Sciences. IRDye800 or IRDye680 secondary antibodies were purchased from LI-COR Biosciences. The PKC inhibitor Calphostin C was purchased from R&D Systems. Other reagents were from Sigma or Thermo Fisher Scientific.

Co-immunoprecipitation of EGFR and c-Cbl and Ubiquitylation of EGFR—Cells were serum-starved overnight and incubated with the ligand in HEPES-supplemented DMEM for the indicated time intervals at 37 °C. After incubation, the cells were quickly washed with ice-cold PBS and lysed in buffer containing 1% Triton X-100, 2 mM phenylmethylsulfonyl fluoride, 10 μg/ml aprotinin, 10 μg/ml leupeptin, and phosphatase inhibitors (also supplemented with iodoacetomide (20 mM) if lysates were used for detection of ubiquitylated species) for 1.5 h at 4 °C. The insoluble material was pelleted at 7000 × *g* for 10 min. EGFR was immunoprecipitated with the Ab-12 (anti-EGFR mAb) for 2 h at 4 °C on the rotating wheel, and then the mixture was incubated with protein G-agarose beads for 2 h at 4 °C as before (19). The complexes were eluted from the beads with Laemmli loading buffer. Proteins were resolved in 10% SDS-PAGE, transferred to a nitrocellulose membrane, and developed with the appropriate antibody. Protein bands were visualized using horseradish peroxidase-conjugated goat anti-mouse antibodies (Dako) and chemiluminescence reagent (PerkinElmer Life Sciences) or IRDye800 secondary antibody for detection using the LI-COR Odyssey Imaging System. Production and purification of sΔHB-EGF has been described elsewhere (20, 21).

Detection of Phosphorylated Proteins—Detection of phosphorylated proteins was carried out by Western blotting. The cells were serum-starved overnight and, after incubation with the ligand for indicated time intervals, were lysed with hot Laemmli buffer supplemented with inhibitor mixture as described above. Equal amounts of protein were resolved in 10% SDS-PAGE, transferred to a nitrocellulose membrane, and developed with phospho-specific antibodies.

Inhibitor Treatment—HB2 and HB2/CD82 cells were plated on 6-cm dishes 24 h before the start of the experiment. The cells were serum-starved overnight and treated with 5 μM Calphostin C for 1.5 h. Subsequent incubation with HB-EGF was carried out in the presence of the inhibitor. Appropriate concentration of the drug was determined in a pilot experiment.

Measurement of Changes in Surface Levels of EGFR by Flow Cytometry—The cells were incubated on ice with growth factors for 1 h, then washed, and transferred to 37 °C for the indicated time intervals. After incubation, they were quickly transferred to ice, washed with ice-cold PBS, detached on ice with

Downloaded from http://www.jbc.org/ at OSAKA UNIVERSITY on May 1, 2014

EDTA, incubated with primary antibodies for 45 min on ice, washed twice with wash buffer (0.1% heat-inactivated BSA/PBS), and then labeled with FITC-conjugated goat anti-mouse IgG for 45 min on ice. After two washes, the cells were fixed with 2% paraformaldehyde and analyzed using Coulter Epics program (Becton Dickinson).

Immunofluorescence—The cells were grown on glass coverslips in complete medium for 24–36 h, serum-starved overnight, and incubated with ligand (and/or mouse monoclonal antibody against CD82 (TS82b)) for the indicated time intervals. After incubation, the cells were fixed with 2% paraformaldehyde/PBS for 10 min and, if necessary, permeabilized with 0.1% Triton X-100/PBS for 2 min. Staining with primary and fluorochrome-conjugated secondary antibodies was carried out as previously described (22). The images were captured using Zeiss LSM510 META confocal system with 63× oil immersion objective (NA 1.4). Z-stack sections were collected at 0.3–0.4-μm intervals. Quantification of co-localization was carried out on 40–50 cells from two or three experiments using ImageJ Plugin JACOP (23).

Microplate Internalization Assay—The cells were plated on 96-well flat-bottomed plates at the density 5×10^3 cells/well, 6 wells for each time point. After 48 h, the cells were washed three times with ice-cold PBS and incubated with the primary antibody (anti-CD82 mAb, TS82b) at 4 °C for 1 h. Three washes with PBS were followed by incubation at 37 °C in full medium for various time intervals. Then cells were fixed with 2% paraformaldehyde for 10 min, blocked with 1% heat-inactivated BSA in PBS, and incubated with IRDye 800CW goat anti-mouse IgG from LI-COR Biosciences. After three washes with PBS, the plates were dried, and fluorescence was quantified in 800-nm channel by the Odyssey Infrared Imaging System (LI-COR Biosciences). Experiments were carried out at least three times. Statistical significance was calculated by paired, two-tailed *t* test.

Electron Microscopy—For immunoelectron microscopy, cells were fixed in 2% paraformaldehyde, 0.125% glutaraldehyde (Sigma-Aldrich) in 0.2 M phosphate buffer (pH 7.4) and recovered from the culture plates using cell scrapers. The cells were embedded in 10% gelatin and infused with 2.3 M sucrose as described previously (24, 25). Gelatin blocks were frozen in liquid nitrogen, and ultrathin sections were collected on drops containing a mixture of methylcellulose and sucrose (25), deposited on Formvar carbon-coated copper grids and single- or double-immunogold labeled using indicated antibodies and protein A coupled to 10- or 15-nm gold particles. Protein A-conjugated 10- or 15-nm gold particles (PAG10 or PAG15) were purchased from the microscopy center of Utrecht University (Utrecht, the Netherlands). Grids were contrasted/embedded in 0.4% uranyl acetate, 1.8% methylcellulose and dried. For conventional electron microscopy with pre-embedding labeling, cells grown on coverslips were incubated with anti-CD82 mAb (TS82b or IA4) at 4 °C for 1 h. After three washes (to remove unbound antibody), the cells were incubated with protein A coupled to 10-nm gold particles at 4 °C for 1 h. After three washes (to remove unbound gold particles), the cells were chased at 37 °C in full medium for the indicated time intervals. The cells were then fixed with 2.5% glutaraldehyde in 0.1 M cacodylate buffer for 90 min, post-fixed with 2% OsO4, dehydrated in ethanol, and embedded in Epon. Ultrathin (60–70 nm) sections were examined using a Philips CM120 electron microscope (FEI Company, Eindhoven, the Netherlands) equipped with a digital camera Keen View (OSIS, Münster, Germany).

RESULTS

HB-EGF-induced Ubiquitylation of EGFR Is Impaired in Cells with High Expression Level of CD82—EGF receptor signaling potential depends on a delicate balance between processes of recycling and degradation. The fate of the receptor is decided in sorting endosomes following ligand-induced internalization. One of the critical regulatory mechanisms of intracellular trafficking of the activated EGFR is ubiquitylation (17). Following earlier reports describing the role of CD82 in EGF-induced internalization of EGFR (5, 12), we investigated whether ligand-induced ubiquitylation of the receptor is influenced by this tetraspanin. We examined three ligands (EGF, AR, and HB-EGF) that are known to induce different levels of ubiquitylation and have distinct effects on the postendocytic trafficking of EGFR (26). Cells with low or high levels of CD82 (Fig. 1*A*) were serum-starved overnight, and kinetics of ubiquitylation of EGFR in response to the ligands were investigated after a chase with a ligand for up to 30 min at 37 °C. Stimulation of the control cells (HB2) with EGF and HB-EGF induced robust ubiquitylation of EGFR (Fig. 1, *B* and *C*, *lanes 1–5*), reaching the maximum at 5–15 min. Amphiregulin induced weaker ubiquitylation of the receptor with a maximum at 5 min (Fig. 1*D*, *lanes 1–5*). Weaker AR-induced ubiquitylation of EGFR was previously reported and linked to the initiation of higher recycling rate of AR-activated receptor (26, 27).) When the cells with high expression level of CD82 (HB2/CD82) were stimulated with EGF, we observed similar kinetics and degree of EGF-induced ubiquitylation of the receptor (Fig. 1*B*, *lanes 6–10*). By contrast, ubiquitylation of EGFR stimulated with either HB-EGF or AR was markedly impaired (2–3-fold, depending on ligand and time point) in HB2/CD82 cells when compared with control cells (Fig. 1, *C* and *D*, *lanes 6–10*). These data were further confirmed when we used different concentrations of EGF and HB-EGF for stimulation (supplemental Fig. S1).

To provide further evidence that HB-EGF-induced ubiquitylation of EGFR is, indeed, regulated by CD82, we used shRNA approach to selectively deplete CD82 in 2.5.2A breast cancer cells. Ubiquitylation of HB-EGF-stimulated EGFR in CD82-depleted cells increased (up to 3-fold) when compared with parental cells (Fig. 2*A*), confirming the role of CD82 in modulation of EGFR ubiquitylation. 2.5.2A cells express EGFR at a similar level to HB2 cells but have higher expression levels of CD82 (Fig. 1*A* and 2*B*).

Two ligands (HB-EGF and AR) that cause CD82-dependent decrease in ubiquitylation of EGFR contain heparin-binding domain, and we have previously reported that the activity of HB-EGF is controlled by its heparin-binding (HB) region via interaction with heparan sulfate proteoglycans (HSPG) (20). Thus, we examined whether HB domain of HB-EGF is essential for changes in the ubiquitylation of the receptor in cells expressing CD82. Notably, ubiqitylation of EGFR in both HB2

Downloaded from http://www.jbc.org/ at OSAKA UNIVERSITY on May 1, 2014

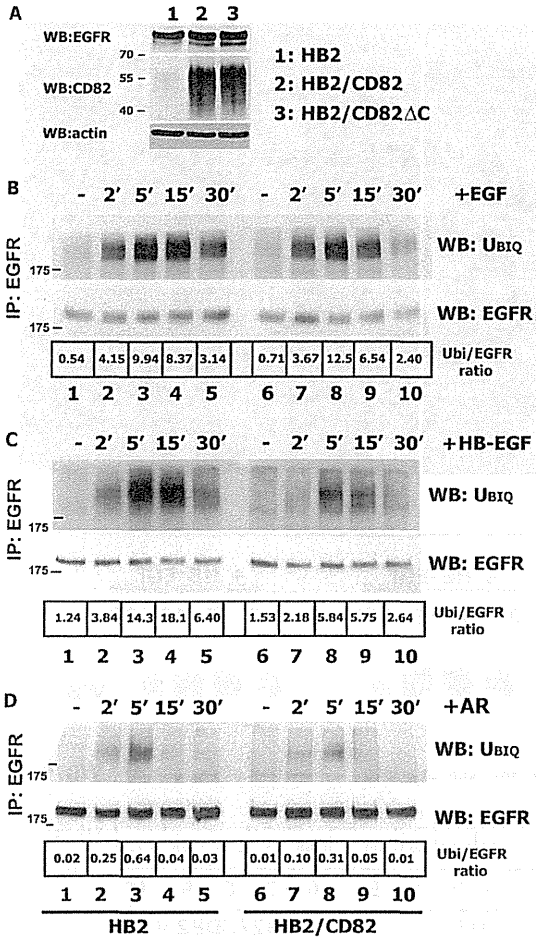

FIGURE 1. **Ubiquitylation of EGFR is impaired in CD82-overexpressing cells.** *A*, expression levels of CD82 and EGFR in HB2, HB2/CD82, and HB2/CD82ΔC cells were determined by Western blotting (*WB*) with anti-CD82 mAb (TS82b) or with anti-EGFR (Ab-15) mAb, respectively. WB with anti-actin mAb is a control for equal loading. *B–D*, HB2 and HB2/CD82 cells were serum-starved overnight and incubated with 15 ηg/ml EGF (*B*) or 20 ηg/ml HB-EGF (*C*) or 15 ηg/ml AR (*D*) for the indicated time intervals. After incubation, the cells were lysed in Triton X-100 (1%), EGFR was immunoprecipitated (*IP*) with anti-EGFR mAb (Ab-12; Neomarkers), and ubiquitylation (*UBIQ*) of the receptor was determined by Western blotting with anti-ubiquitin mAb (FK2; Enzo). The membranes were reblotted with anti-EGFR pAb (Cell Signaling). The results of one of three independent experiments are shown. Densitometric analysis was carried out on the films of equal exposure time using the ImageJ program.

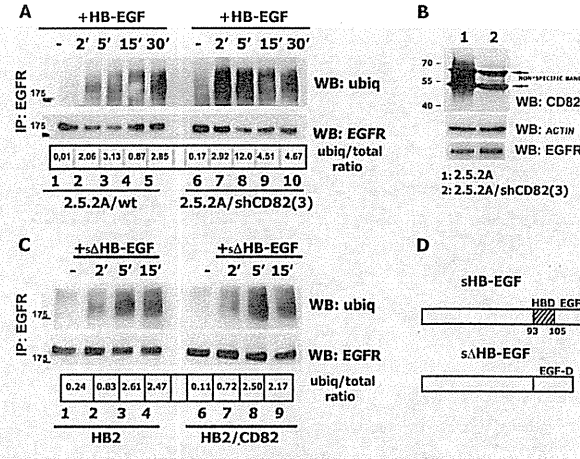

FIGURE 2. **Impairment of ubiquitylation of HB-EGF-stimulated EGFR is dependent on CD82 expression level and heparin-binding domain of the ligand.** *A*, 2.5.2A/wt and 2.5.2A/shCD82 cells were serum-starved overnight and incubated with 25 ηg/ml HB-EGF for indicated time intervals. After incubation, the cells were lysed in Triton X-100 (1%), EGFR was immunoprecipitated (*IP*) with anti-EGFR mAb (Ab-12; Neomarkers), and ubiquitylation (*ubiq*) of the receptor was determined by Western blotting (*WB*) with anti-ubiquitin mAb (FK2; Enzo). The membranes were reblotted with anti-EGFR pAb (Cell Signaling). The results of one of three independent experiments are shown. *B*, expression levels of CD82 and EGFR in 2.5.2A wild type and CD82 knockdown cells were determined by Western blotting with the appropriate antibodies. Equal loading was controlled by WB with anti-actin mAb. *C*, HB2, HB2/CD82 cells were serum-starved overnight, incubated with 10 ηg/ml sΔHB-EGF for indicated time intervals. Ubiquitylation of the receptor was determined by Western blotting with anti-ubiquitin mAb (FK2; Enzo) after immunoprecipitation as described above. The results of one of two independent experiments are shown. *D*, schematic structures of wild type and mutant forms of HB-EGF (adapted from Ref. 21).

and HB2/CD82 cell lines was robust and comparable following stimulation with sΔHB-EGF, HB-EGF with deleted HB domain (Fig. 2, *C* and *D*). The changes in ubiquitylation after stimulation with sΔHB-EGF could not be attributed to the different receptor-binding parameters of the ligand because we have reported earlier that binding of soluble ΔHB-EGF is comparable with that of the wild type (21). The lower total ubiquitylation levels in these experiments were due to the lower concentration of the ligand (10 ηg/ml). Taken together, these data indicate that CD82 selectively regulates ligand-induced ubiquitylation of EGFR through a novel mechanism that possibly involves surface heparan sulfate proteoglycans.

Postendocytic Trafficking of CD82 and Activated EGFR—We expected that CD82-dependent decrease in EGFR ubiquitylation would affect intracellular trafficking of the receptor. Thus, we investigated trafficking of the receptor in HB-EGF-stimulated cells in more detail. It is well established that activated EGFR is initially delivered to the EEA1-positive endosomes (26). Hence, we compared the dynamics of EGFR trafficking through this compartment in HB2 and HB2/CD82 cells after stimulation with HB-EGF. The cells were incubated with ligand on ice for 1 h, then washed, and transferred to 37 °C for indicated time intervals. Then cells were fixed, permeabilized, and labeled for EGFR and EEA1 (Fig. 3*A*). Quantification analysis of the collected z-stacks of images showed that after 2 min of incubation with HB-EGF, the proportion of EGFR co-localized with EEA1 was significantly higher in control cells (Fig. 3*B*) (27% in HB2 and 17% in HB2/CD82 cells). The difference was also observed in cells after 5 min of incubation, although less pronounced (Fig. 3*B*) (37% for HB2/CD82 cells and 30% for the control cells). Maximum (and comparable) co-localization has been reached after 15 min in both cell lines (38 and 43%, respectively) with sharp decline (from 43% to 30%) in HB2/CD82 cells at 30 min (Fig. 3*B*). In contrast, in HB2 cells co-localization of EGFR with EEA1 did not change over the 5–30-min time interval. We conclude that we observed slow delivery of EGFR to EEA1-positive endosomes and fast egress from this compartment in HB2/CD82 cells. In contrast, EGFR in control cells was fast delivered to and retained in EEA1-labeled endosome over the indicated time interval.

We also investigated intracellular trafficking of EGFR in cells expressing CD82ΔC (C-terminal deletion mutant of CD82). Interestingly, recruitment of EGFR to the EEA1-positive compartment at earlier time points in these cells was comparable

Downloaded from http://www.jbc.org/ at OSAKA UNIVERSITY on May 1, 2014

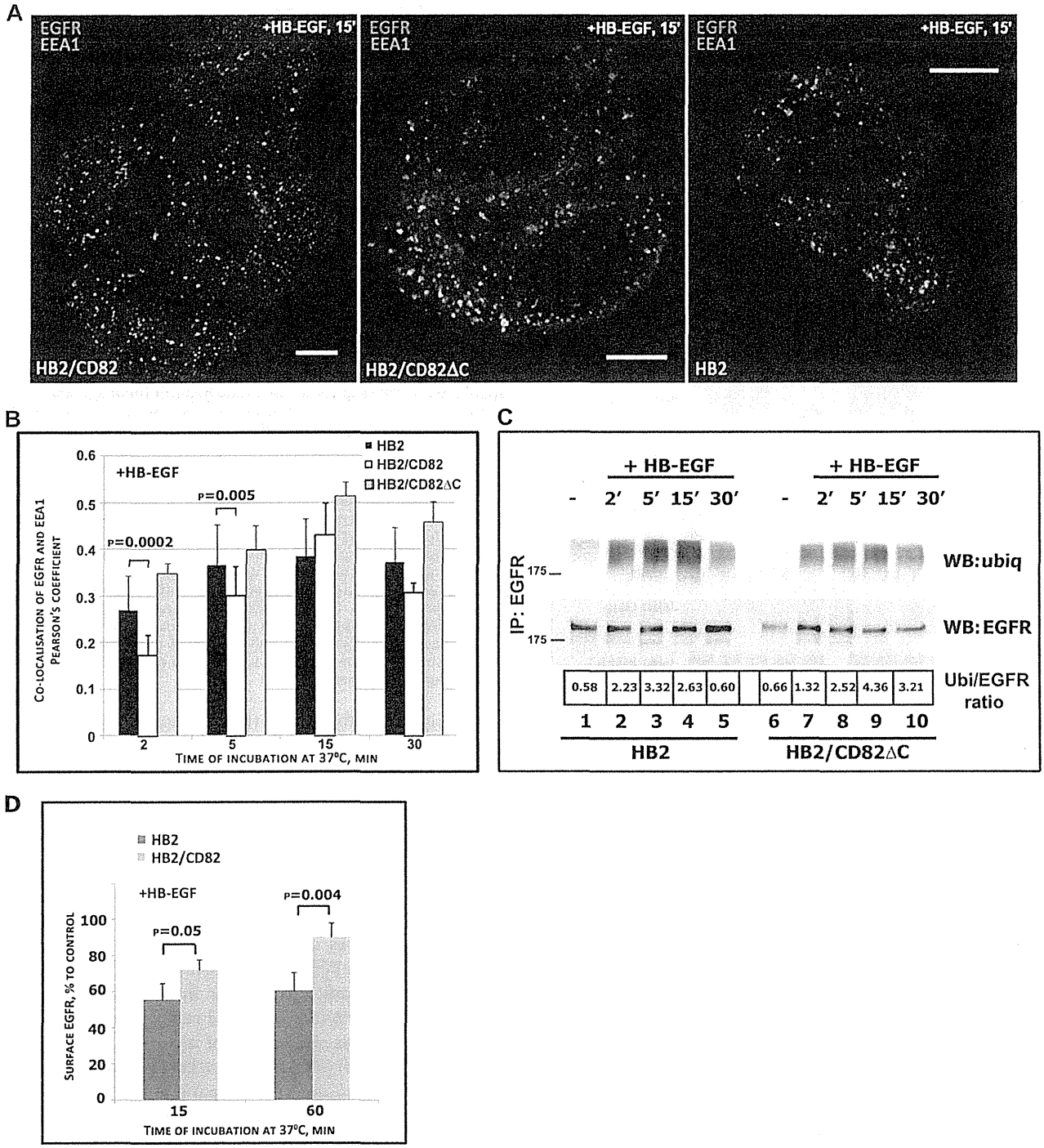

FIGURE 3. **Postendocytic trafficking of EGFR following HB-EGF stimulation is altered in the presence of CD82.** *A* and *B*, HB2, HB2/CD82wt, and HB2/CD82ΔC cells plated on coverslips were serum-starved overnight and incubated with HB-EGF (25 ηg/ml) at 37 °C for indicated time intervals. The cells were fixed and labeled for EGFR (anti-EGFR mAb; Ab-15) and the early endosomal marker EEA1 (anti-EEA1 mAb; Transduction Labs) (as described under "Experimental Procedures"). *A*, Representative confocal images of the cells following 15 min of EGFR internalization. *Bars*, 10 μm. *B*, quantification of the amount of EGFR co-localizing with EEA1 in an average of 40–50 cells for each time point is presented as Pearson's coefficient (average of three experiments). The *p* values were determined by paired two-tailed *t* test. *C*, ubiquitylation (*ubiq* or *Ubi*) of EGFR in HB2 and HB2/CD82ΔC cells was determined by immunoprecipitation (*IP*) as described under "Experimental Procedures." The results of one of three independent experiments are shown. *D*, time course of EGFR recycling in HB2 and HB2/CD82 cells following stimulation with HB-EGF. The cells were incubated on ice with the ligand, washed, and incubated at 37 °C for indicated time intervals. The amount of EGFR at the cell surface was determined by flow cytometry. The values presented are means (percentages) ± S.D. from four experiments. *WB*, Western blotting.

with that seen in control cells (Fig. 3*B*). Thus, deletion of the C-terminal part of CD82 renders this protein inactive toward EGFR in this assay. Because we proposed that CD82-dependent differences in HB-EGF-induced trafficking may be due to decreased ubiquitylation of EGFR, it was important to compare ubiquitylation kinetics in the control and CD82ΔC-expressing

Downloaded from http://www.jbc.org/ at OSAKA UNIVERSITY on May 1, 2014

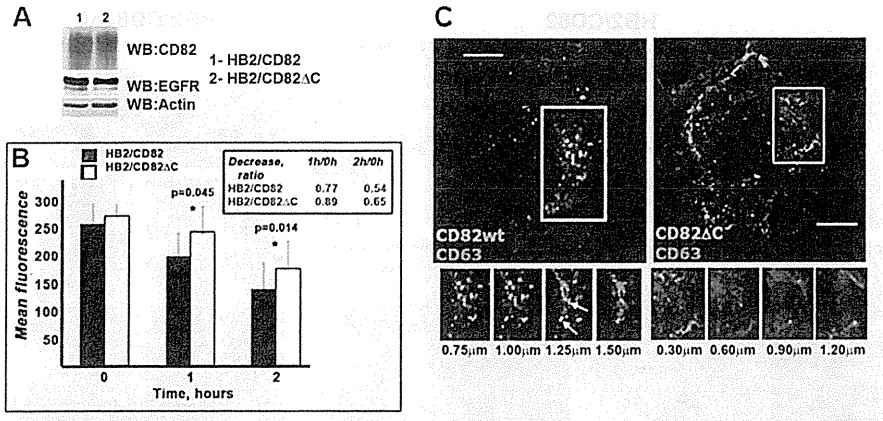

FIGURE 4. **Mutation in C-terminal of CD82 changes intracellular trafficking of the tetraspanin.** *A*, expression levels of CD82wt and CD82ΔC determined by Western blotting (*WB*). *B*, internalization rate of CD82 in HB2/CD82 and HB2/CD82ΔC cells was studied using microplate internalization assay as described under "Experimental Procedures." Internalization of anti-CD82 mAb (IA4 or TS82b) was monitored (after 1 and 2 h of chase at 37 °C) with IRDye 800CW and Odyssey Infrared Imaging System (LI-COR Biosciences). The graph presents average of mean fluorescence values from three experiments (± S.D.) for each cell line at indicated time point. The values presented in the table are ratios at particular time points relative to values at zero time point. The *p* value for each time point was determined in paired two-tailed *t* test. *C*, representative confocal images following uptake of anti-CD82 mAb (IA4) after 1 h of chase in cells expressing CD82wt or CD82ΔC are shown. The cells were acid-washed, fixed, permeabilized, and co-stained with anti-CD63 (1B5) mAb (as described under "Experimental Procedures"). Co-localization of CD82 and CD63 was assessed using isotype specific Alexa Fluor-conjugated goat anti-mouse antibodies. Z-sections were taken at the interval of 0.30–0.35 μm. *Scale bar*, 10 μm.

cells. As illustrated in Fig. 3*C*, HB-EGF-induced ubiquitylation of EGFR in HB2/CD82ΔC cells was even increased when compared with HB2 cells. Taken together, these data show that CD82-dependent attenuation of EGFR ubiquitylation in cells stimulated with HB-EGF correlates with the delayed recruitment of the receptor to EEA1-positive endosomes and accelerated egress from these compartments. Importantly, this activity of CD82 is dependent on the cytoplasmic C-terminal part of the protein.

Decreased ubiquitylation and changed dynamics of recruitment to early endosomes may be an indication of the receptor's diversion to a recycling route. We compared cell surface levels of EGFR after HB-EGF stimulation in HB2 control and HB2/CD82 cells as measured in pulse-chase experiments by flow cytometry (Fig. 3*D*). In accordance with the ubiqitylation data described above, the number of HB-EGF-activated receptors on the cell surface in HB2/CD82 cells was higher than in control cells (15 min after stimulation). Furthermore, after 60 min incubation with HB-EGF the number of receptors was increased. Although the newly synthesized receptors were not taken into account in these experiments, the number would not be greatly changed because of a relatively short time course. Taken together, these data clearly indicate that CD82 expression alters trafficking routes of HB-EGF-stimulated EGFR.

Trafficking of CD82 Is Controlled by the C-terminal Cytoplasmic Domain of the Protein—The C-terminal cytoplasmic region deleted in CD82ΔC mutant contains a classical tyrosine-based sorting signal (YSKV). As we have described above, its deletion negated effects of CD82 on the ubiquitylation and intracellular trafficking of EGFR.

Thus, it was important to compare trafficking routes of CD82wt and CD82ΔC from the plasma membrane in more detail. Initially, we measured the rate of the mAb-induced internalization of CD82 using a microplate internalization assay in cells stably transfected with CD82wt or CD82ΔC (the expression levels of both proteins were comparable; Fig. 4*A*). The internalization rate of antibody-bound CD82wt was slow with only ~23% of CD82wt being removed from the cell surface after 1 h of chase (Fig. 4*B*). After 2 h of chase ~54% of CD82wt could still be detected at the cell surface. Internalization of antibody-bound CD82ΔC appeared to be even slower with only ~11% of the protein being removed after 1 h and ~35% being removed after 2 h (Fig. 4*B*). Immunofluorescence analysis of the internalized CD82 at the 1-h time point following anti-CD82 mAb binding illustrated the difference in the distribution patterns of CD82wt and CD82ΔC (Fig. 4*C*). The wild type protein was found in round puncta in perinuclear area (Fig. 4*C*, *left panel*). On the other hand, internalized CD82ΔC was found in the CD63-negative "polymorphic" structures close to the plasma membrane (Fig. 4*C*, *right panel*).

We also studied the distribution of internalized CD82wt and CD82ΔC between various intracellular compartments by electron microscopy. We used two different approaches: immunogold labeling of cryosections prepared from the cells after antibody chase and EPON embedding of the samples after chase with antibody-bound gold. The images from the second set of experiments are shown because they are more illustrative. After 5 min of chase at 37 °C, gold-labeled CD82 was found at the plasma membrane (Fig. 5*A*, *arrows*) and in the uncoated invaginations of plasma membrane (PM) (Fig. 5*B*, *arrows*). Interestingly, CD82 was not detected in coated invaginations of the PM (Fig. 5*C*, *arrowheads*), but it was found on the uncoated internal vesicles (Fig. 5*C*, *arrows*). CD82 could often be detected in the rosette-like endosomal structures, thereby highlighting the diversity of CD82 trafficking pathways (Fig. 5, *D*, *arrows*, and *K*). After a 60-min chase, CD82 was distributed in various multivesicular endosomes at different stages of biogenesis and at the PM (Fig. 5, *E* and *F*, *arrows*). Occasionally, gold-labeled CD82 was found on extracellular vesicles (Fig. 5*F*). Lack of a visible coat and the morphology of the PM invaginations labeled for CD82, together with the data from siRNA knockdown experi-

Downloaded from http://www.jbc.org/ at OSAKA UNIVERSITY on May 1, 2014

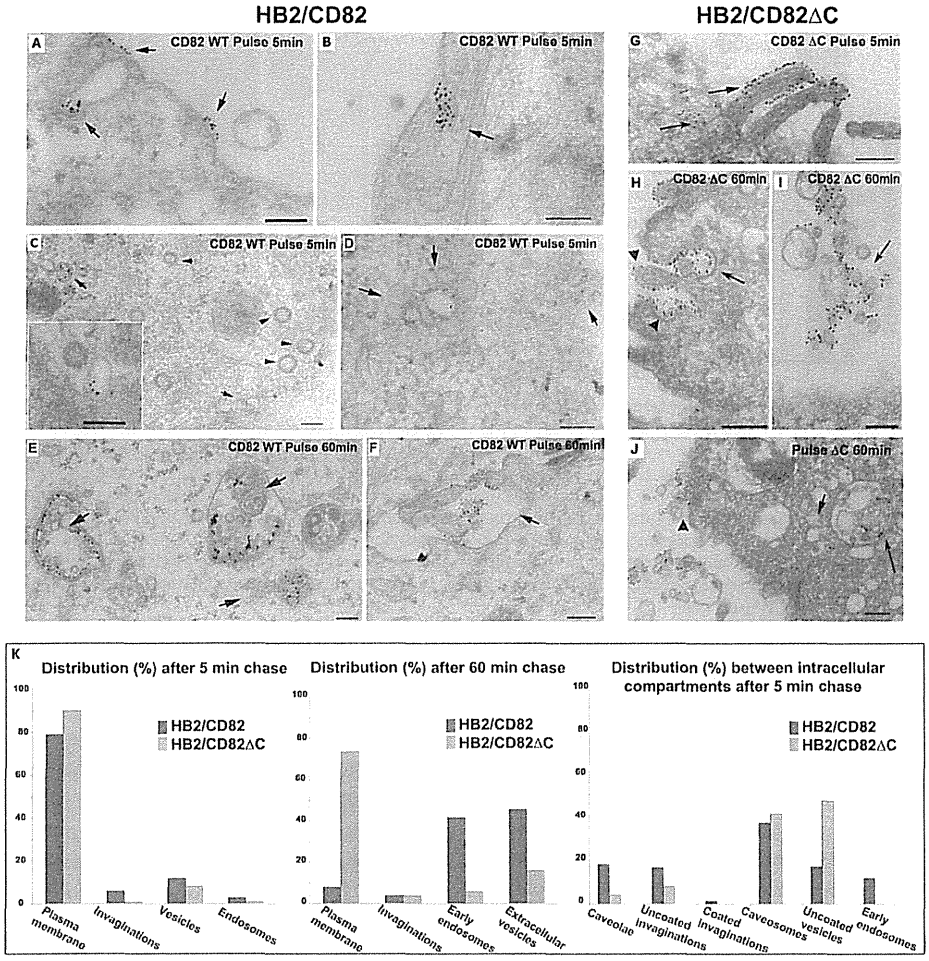

FIGURE 5. **Distribution of CD82 after 5 and 60 min of chase with anti-CD82 mAb analyzed by electron microscopy.** HB2/CD82wt and HB2/CD82ΔC were incubated with anti-CD82 mAb (TS82b) for 1 h and then with protein A gold 10 nm for 40 min at 4 °C and subsequently chased for 5 or 60 min at 37 °C. Then the cells were fixed and processed according to the protocol described under "Experimental Procedures." *A*, *B*, and *G*, after 5 min of chase, CD82wt and CD82ΔC were distributed to the plasma membrane and in the uncoated invaginations of PM. *C* (*main panel* and *inset*), after 5 min of chase, internalized CD82wt was found in the uncoated structures (*arrow*) but not coated vesicles (*arrowheads*). *D*, after 5 min of chase, CD82wt was observed in rosette-like endosomal structures. *E*, after 60 min of chase, internalized CD82wt was mainly distributed to the intracellular multivesicular compartments (*arrows*) and found occasionally at the PM. *F*, after 60 min of chase, gold-labeled CD82wt was also found on extracellular vesicles (*arrows*). *H–J*, CD82ΔC after 60 min chase was found on internal (*H* and *J*) and on extracellular (*I*) vesicles. *K*, quantification of the distribution of gold particles (average 1500) between various membranous compartments after 5 and 60 min of chase with anti-CD82 mAb in HB2/CD82wt and HB2/CD82ΔC cells. *Scale bar*, 200 nm.

ments of AP-2 (data not shown), excluded involvement of clathrin-coated pits in the internalization of CD82.

Similarly to the wild type, after a 5-min chase, the C terminus deletion mutant of CD82 (CD82ΔC) was found mainly at the cell surface and in the uncoated invaginations (Fig. 5*G*, *arrows*). At a later time point (60 min), CD82ΔC was occasionally found in multivesicular endosomes/lysosomal structures with enlarged internal vesicles (Fig. 5, *H* and *J*, *arrows*) and on the extracellular vesicles (Fig. 5*I*, *arrow*), but it was mainly distributed at the PM (Fig. 5, *H* and *J*, *arrowheads*). Study of the intracellular morphology and quantification of immunogold labeling data confirmed that the C-terminal cytoplasmic domain is involved in the postendocytic sorting and intracellular trafficking of CD82 (Fig. 5*K*). Compartmental distribution of CD82 and CD82ΔC after internalization was profoundly different (Fig. 5, *A–K*).

Having established the importance of the C-terminal cytoplasmic region in trafficking of CD82, we next examined the co-trafficking of EGFR and CD82 after stimulation with HB-EGF. To follow trafficking of the receptor in relation to the surface pool of CD82, these experiments were performed in the presence of anti-CD82 mAb (we found that the presence of this antibody did not affect ligand binding to EGFR or did not alter receptor-mediated signaling (not shown)). Cells were incubated with the ligand and antibody on ice for 1 h, then washed, and incubated at 37 °C for various time intervals. We observed partial co-localization of internalized EGFR and CD82 proteins at all time points: the receptor and tetraspanin were detected in vesicles localized in close proximity to the plasma membrane and in the perinuclear region (Fig. 6*A*). The quantification analysis of confocal images demonstrated a substantial degree of co-localization of the internalized receptor and the wild type CD82 throughout the 60-min chase: the difference in co-localization between the first and last time points was ~13% (Fig. 6*B*). Notably, the co-localization for the EGFR-CD82ΔC pair in a similar assay

Downloaded from http://www.jbc.org/ at OSAKA UNIVERSITY on May 1, 2014